TRANSPORTATION RESEARCH BOARD
NATIONAL RESEARCH COUNCIL

IDEA

Innovations Deserving Exploratory Analysis Project

NATIONAL COOPERATIVE HIGHWAY RESEARCH PROGRAM

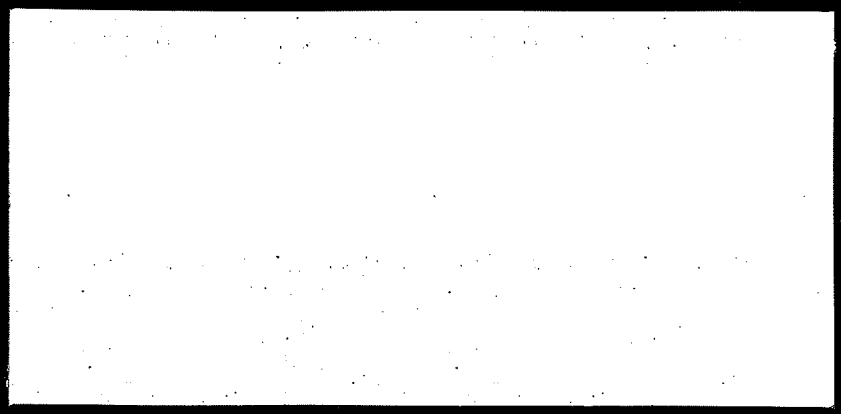

Report of Investigation

IDEA PROJECT FINAL REPORT

Contract NCHRP-94-IDO14

IDEA Program
Transportation Research Board
National Research Council

March 1997

UNREINFORCED, CENTRALLY PRESTRESSED COLUMNS AND PILES

Prepared by:
D.V. Reddy,
Florida Atlantic University
Boca Raton, Florida
Paul Csagoly
Consultant
Clearwater, Florida

INNOVATIONS DESERVING EXPLORATORY ANALYSIS (IDEA) PROGRAMS
MANAGED BY THE TRANSPORTATION RESEARCH BOARD (TRB)

This NCHRP-IDEA investigation was completed as part of the National Cooperative Highway Research Program (NCHRP). The NCHRP-IDEA program is one of the four IDEA programs managed by the Transportation Research Board (TRB) to foster innovations in highway and intermodal surface transportation systems. The other three IDEA program areas are Transit-IDEA, which focuses on products and results for transit practice, in support of the Transit Cooperative Research Program (TCRP), Safety-IDEA, which focuses on motor carrier safety practice, in support of the Federal Motor Carrier Safety Administration and Federal Railroad Administration, and High Speed Rail-IDEA (HSR), which focuses on products and results for high speed rail practice, in support of the Federal Railroad Administration. The four IDEA program areas are integrated to promote the development and testing of nontraditional and innovative concepts, methods, and technologies for surface transportation systems.

For information on the IDEA Program contact IDEA Program, Transportation Research Board, 500 5th Street, N.W., Washington, D.C. 20001 (phone: 202/334-1461, fax: 202/334-3471, http://www.nationalacademies.org/trb/idea)

UNREINFORCED, CENTRALLY PRESTRESSED COLUMNS AND PILES

TABLE OF CONTENTS

EXECUTIVE SUMMARY

It has been observed that the compressive resistance of axially-loaded reinforced concrete components is invariably less than the sum of individual strengths of the constituent concrete and steel elements due to structural incompatibility in the inelastic phase. Accurate prediction of their resistance is difficult due to structural instability that takes place at or near ultimate limit states in traditionally reinforced concrete columns. This unreliability, exacerbated by the fact that loading columns without eccentricity is practically impossible, causes design codes to specify severe resistance factors in order to assure a desirable safety level. Structural reliability is further impaired by the probability of spalling of the concrete cover due to corrosion of reinforcement.

Part I of this project deals with the nature of compressive fracture mechanism of short, unreinforced concrete columns. Tests indicate that failure of unrestrained concrete is shear-tensile in nature, and that the inclination of fracture plane is independent of the shape of the specimen, but becomes slightly steeper as the compressive strength increases. The geometry of the standard compressive test cylinder is believed to cause unconservative measures for high strength concrete.

Part II consists of a series of tests in which the performance of the Centrally Prestressed Unreinforced Concrete (CPUC) column is compared with that of traditionally constructed bridge piers and piles. The CPUC column design is the first innovative idea of this project by which the innate incompatibility between concrete and steel is eliminated through removal of the latter; flexural resistance and ductility are restored by the application of a centrally located prestressing tendon or closely spaced strands. This concentration of steel results in a significant increase in concrete cover for better corrosion protection without loss in strength.

Part III entails physical experimentation relative to a steel-concrete component, which is structurally compatible with the CPUC column, and provides a level of ductility unattainable by any other known concrete column design. Called an Extended Performance Flexural (EPF) device, it constitutes the second innovative idea in this project. The EPF device enables the CPUC columns to mitigate and safely withstand repetitive force effects generated by severe seismic action, while its broad pseudo-elastic range is capable of satisfying service limit state criteria.

CLAIMS

1. The EPF device has been invented, and is the intellectual property of Paul F. Csagoly.
2. A new shear-tensile fracture model and exponential stress-strain relationship, to which references are made herein, do not constitute parts of this project.

BACKGROUND

DEVELOPMENT AND DESIGN OF PIERS

Early bridges in the United States were supported by wooden trestles and pile groups, but their fast and unarrestable decay mandated the use of fitted stonework, the only reliable and long-lasting structural material available at that time, of which the most magnificent example is the Brooklyn Bridge. As stonework cannot take tension, these piers resist lateral forces by their weight and geometry. Many such piers, with their superstructures long removed, stand abandoned in rivers, waiting for natural degradation that often does not occur.

Mining and transportation of the stones, and the high-precision work required to fit them together, made these piers slow and expensive to build; with the commercial availability of cementitious materials, they have been replaced by cast-in-place concrete piers. As the tensile strength of the concrete had prudently been ignored, replacement was basically one-to-one in terms of geometry and weight. The service life of these piers proved to be not dissimilar to that of natural stone, testifying to the superior qualities of unreinforced concrete.

With the introduction of vertical reinforcement permitting a considerable reduction in size, the pier evolved into a slender column, capable of resisting both axial load and flexure. While many laboratories are equipped to test full-size bridge girders and beams, the sheer size and strength of columns normally preclude such endeavors. Bridge columns are, therefore, always tested as small-scale models, subject to suspicion due to scale effects. Nevertheless, early short-term tests indicated premature loss of cover and subsequent buckling of the vertical bars. The introduction of transverse steel, in the form of spirals for round columns and ties for rectangular columns, had largely resolved the buckling problem, in addition to enhancing the shear strength of the column and providing confinement for the core concrete. Long-term tests revealed a tendency of the concrete to de-stress itself and transfer compressive stresses, due to creep and shrinkage, to the steel, and to the extent of developing regularly spaced annular cracks, especially in highly reinforced units.

There is an innate incompatibility of materials in the inelastic phase which causes the compressive resistance of axially-loaded reinforced concrete components to invariably be less than the sum of individual strengths of the constituent concrete and steel elements. The problem is further compounded by involuntary eccentricity of the axial load, both in the laboratory and in the field. For instance, peak stress doubles in the elastic phase where the eccentricity is as small as one-sixth of the column dimension.

In order to assure an adequate level of safety, design codes specify severe (i.e. low) reduction factors to determine factored resistance, P_R. The LRFD-based AASHTO Bridge Specifications prescribe the following:

for columns with spirals: $P_R = 0.75 \times 0.85\ [0.85\ f_c'A_c + f_yA_s]$
for columns with ties: $P_R = 0.75 \times 0.80\ [0.85\ f_c'A_c + f_yA_s]$.

One way of interpreting these equations is that the concrete is being discounted as a function of the amount of steel present. For a 24.0 in. square column with $f_c' = 4.0$ ksi and $f_y = 60.0$ ksi, if compared with a solid steel column of cross section A_s and resistance factor of 0.9 as specified, the following discounts can be computed:

1.0% steel: discount 53.5%.
4.5% steel: discount 70.2%.
8.0% steel: discount 88.1%.

The code equations reflect that the reinforced-concrete column, as we know it, is a highly unreliable structural component; they certainly represent a conservative view. However, even this conservative design approach cannot protect the columns against corrosion and earthquake action.

CORROSION IN PIERS

A majority of bridge piers in the United States are exposed to either natural salts in brackish waters or waters laden with deicing salts, which splash and spray on them or percolate through open or leaking deck joints. Chloride ions penetrate the concrete and accelerate corrosion of the steel therein when a threshold concentration level is reached. Presently, corrosion is being considered as the most critical issue in highway bridges.

The mechanics of chloride ion penetration is approximated by Fick's Second Law in one dimension:

$$D(x,t)\ \frac{\partial_2 C}{\partial x^2} = \frac{\partial C}{\partial t}$$

where: $D(x,t)$ = diffusion coefficient (in^2/yr)
$C(x,t)$ = chloride concentration (lb/c.yd)
x = distance from exposed surface (in)
t = time in years.

Ranade and Reddy (1994) extended the previous equation to take into account the two-dimensional nature of chloride diffusion in columns where D is constant, as follows:

$$\frac{\partial C}{\partial t} = D\left(\frac{\partial^2 C}{\partial^2 x} + \frac{\partial^2 C}{\partial y^2}\right)$$

and they developed a solution in the form of:

$$C(x,t) = (4\pi Dt)^{-n/2} \int f(x')e^{-\frac{(x-x')^2}{4Dt}} dx^1$$

For the corner of the component as indicated in Figure 1, the time-dependent chloride diffusion, C_t, was calculated as shown in Figures 1 and 2.

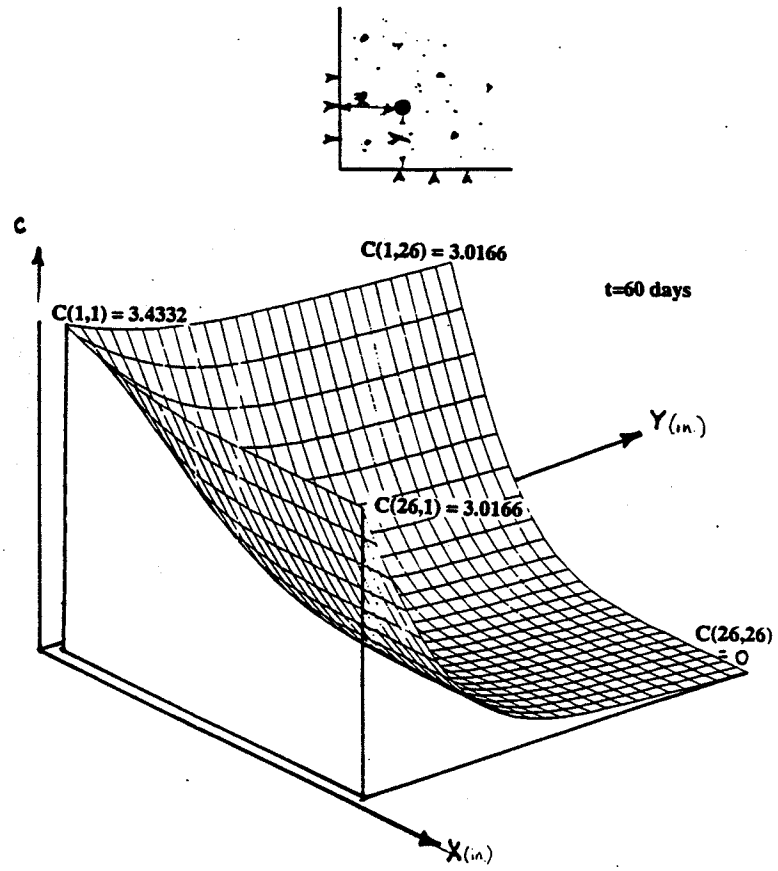

FIGURE 1 Chloride concentration profile.

Formatively, the differential equations are similar to that of heat transfer, meaning that if enough time is given, the concentration will attain the level prevailing at the exposed surface(s). Normally, the distribution or profile of chloride concentration is established experimentally. One such profile, provided by the Florida DOT (FDOT) Materials Laboratory at Gainesville, is shown in Figure 3. Such profiles can be expressed as:

$$C(x,t) = C_s F_{(u)}$$

where:

C_s = concentration at exposed surface
F = non-dimensional function of u
$u = \sqrt{D.t}\ /x$, non-dimensional variable.

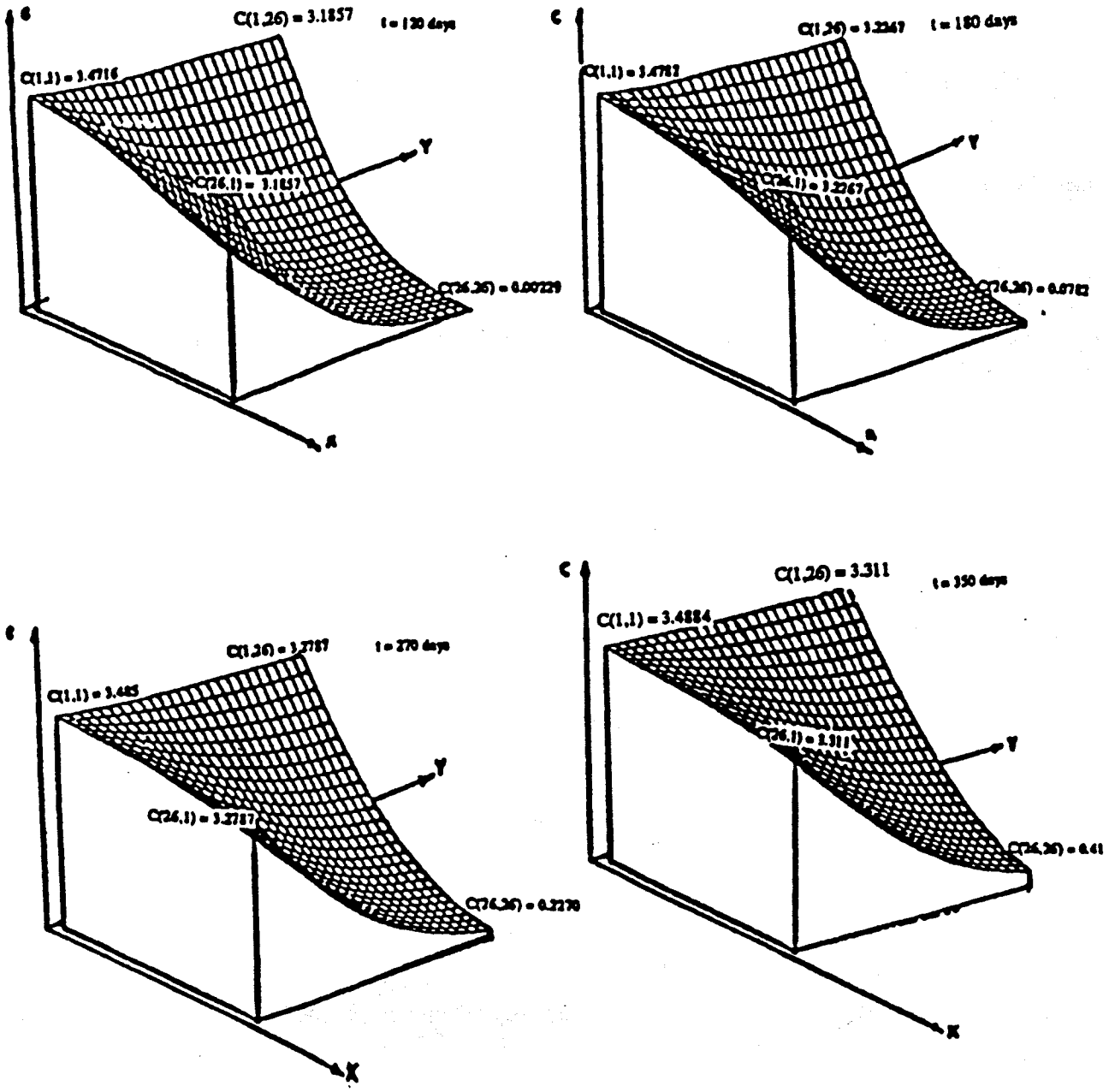

FIGURE 2 Chloride concentration profiles for different times.

It is reported that, in marine structures, the continuous splash-and-wash action seems to maintain a relatively constant C_s = 20.0 lbs/c.yd surface concentration. It is believed that in piers exposed to percolation through deck joints, this value could be much higher.

The objective of corrosion protection is to decelerate or to delay the chloride penetration such that the threshold concentration level is not reached at the steel during the service life of the bridge. There are three ways of doing that:

1. controlling surface concentration C_s by eliminating deck joints, removing salted snow, washing the concrete surface by fresh water and surface sealing;
2. using mixes which produce concretes with high pH and low D values; and
3. increasing the concrete cover x.

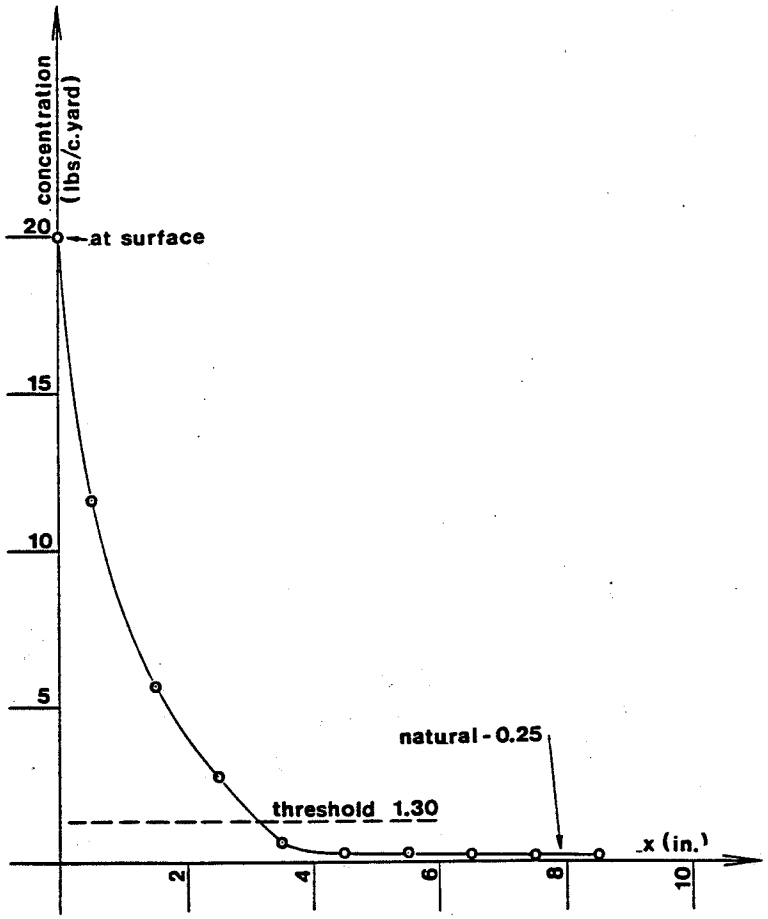

FIGURE 3 Typical chloride concentration profile (FDOT).

The Florida DOT does not consider epoxy coating of steel to be effective corrosion protection, and forbids its use. FDOT has many bridges standing in sea water, and applies no road salts, therefore, Solution 1 above is not applicable, except for surface sealing. However, this is expensive, requires extensive quality control, and is vulnerable to damage and solvents. Recently, there has been considerable progress in producing concretes with low D values, but it is not sufficient. The total solution to corrosion must include the increase of cover, and this approach will be pursued herein.

EARTHQUAKE EFFECTS

In contrast to relatively steady loads, such as dead and live loads, and earth and wind pressures, the earthquake force effect is generated by the mass and stiffness of the structure in response to ground acceleration. Typically, peak ground accelerations last 20 to 40 milliseconds, not dissimilar to collision loads. The magnitude of earthquake force effects is related to the resonance between structural and ground motions; therefore, the best defense against earthquake damage is to increase the period of the fundamental structural vibration mode—significantly above those for observed accelerations. Modern structural design codes determine an equivalent static load as a function of this period of vibration.

In many high-rise buildings, supported by a multitude of relatively flexible columns, this purely structural defense strategy works well. If not, the missing flexibility can be provided by seismic isolators, by which the columns are interrupted, permitting free rotation and/or translation. In bridge structures, economy dictates that the number of columns be kept to a minimum, which, for the relatively high gravitational loads and restricted geometry, usually produces short and heavy pier columns, for which the flexibility strategy fails to work. At this point, no universally

acceptable bridge isolator is available, and in any case, they do not work with single column piers where they would most be needed.

Based on the pictorial evidence resulting from the recent Northridge and Kobe earthquakes, the following failure sequence of spiral reinforced single columns may be reconstructed:

1. By the end of the first half cycle of ground acceleration, the structure develops huge lateral forces due to its stiffness.
2. On the compression side, at the point of maximum moment, the concrete cover is shed, as shown in Figure 4.
3. Upon reversal of acceleration, the concrete cover on the other side is also shed.
4. Because of the scalloped nature of the concrete fracture surface, there is virtually no bond left for the spiral, and the bond for the vertical reinforcement is also reduced.
5. If the spiral is over-lap spliced, the lack of bond causes its unwinding. This also permits the upward and downward sliding of the spiral in the critical area, leading to the buckling of the vertical steel.
6. The instability of steels stops providing confinement for the core concrete which crumbles and spills through the windows thus created in the steel cage.
7. If the splice in the vertical steel is located at the point of maximum moment (Kobe), as usual, crumbling of the core concrete may cause slip in that splice.

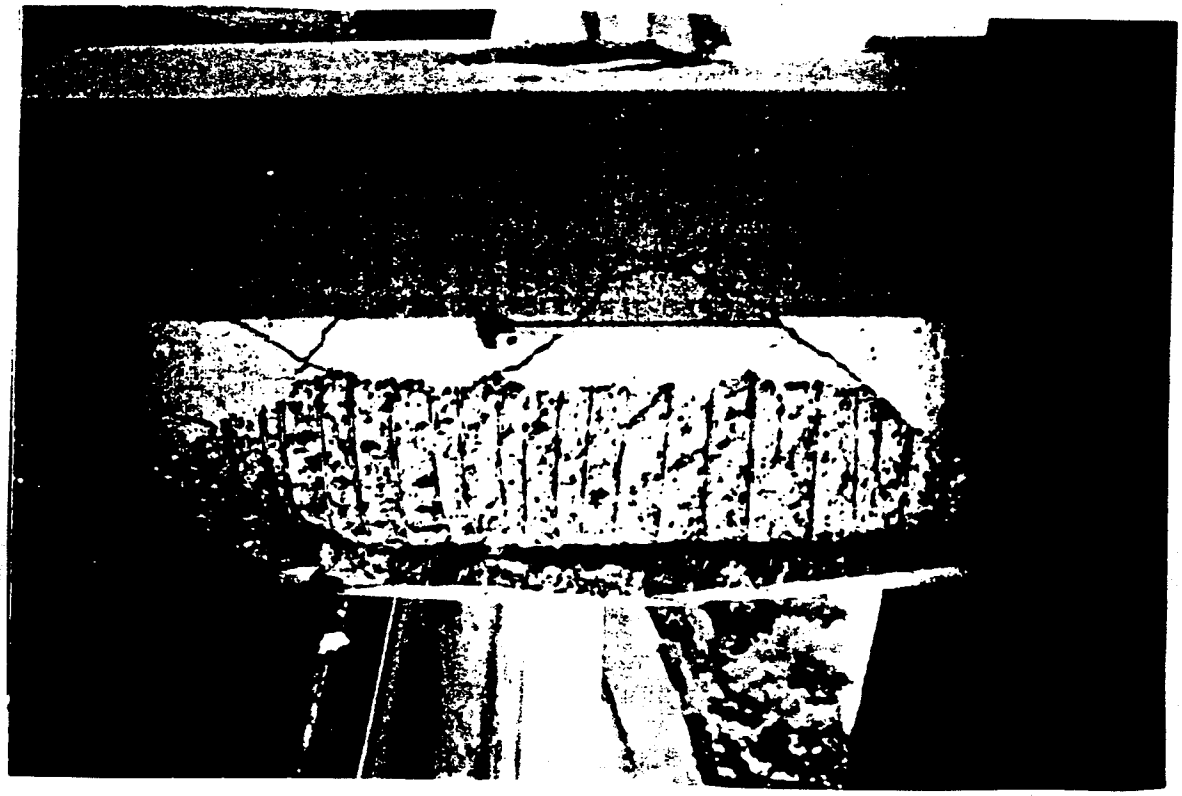

FIGURE 4 Loss of concrete cover (CALTRANS).

A structural effort to increase flexural resistance of the column by adding haunches proved to be counter-productive in the Northridge Earthquake, as the haunched column generated higher forces and the point of destructive action simply moved to the toe of the haunch as illustrated in Figure 5. Currently, a huge rehabilitation program is underway in the State of California, which entails either the passive or active confinement of existing columns. This method of rehabilitation is quite effective, perhaps the best there is, although at least one such confined column is reported to have failed in the Northridge earthquake. The objective of this project is to provide a new column design that can resist earthquake forces without damage in the absence of seismic isolators and artificial confinement.

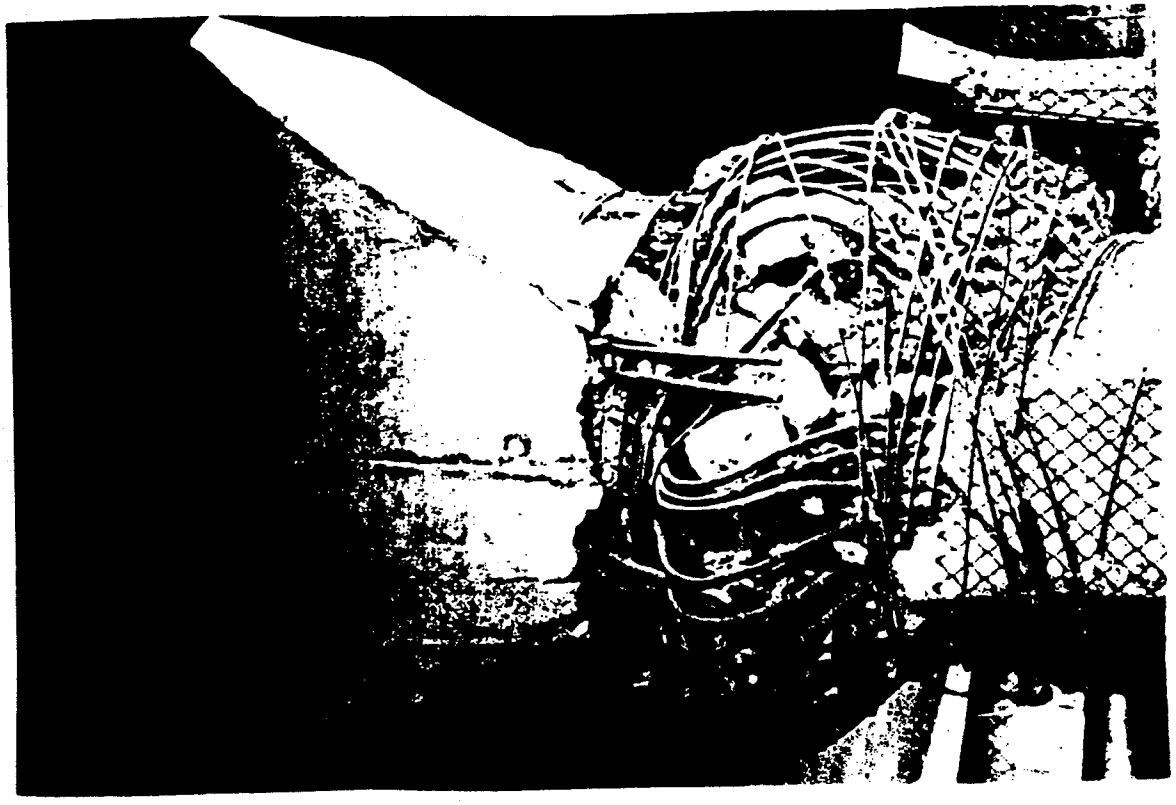

FIGURE 5 Typical reinforced concrete column failure (CALTRANS).

DEVELOPMENT OF INNOVATIVE IDEAS

FLORIDA DOT MODEL TESTS

While employed by the Florida DOT, Paul Csagoly performed a number of compressive tests for an investigation having no bearing on this project. The tests were carried out on standard 6"x12" cylinders, and plain and reinforced 6"x 6"x 30" column stubs of 6,000 psi nominal strength. The specimens were of the same batch of concrete, moist-cured under temperature control in accordance with ASTM specifications. The measured compressive strength at 28 days, the average of four cylinders, was 7,850 psi. The stub tests brought about a number of surprises which were, at that time, ignored basically on the grounds of "too small sample size". They were:

1. The average strength of the unreinforced stubs was 7,490 psi, or 95.7% of the cylinder strength. While the 4.3% difference is well within the expected statistical variation, it is far less than the 15.0% reduction specified for all concretes at the strength limit state.
2. The failure of all the unreinforced stubs occurred in a lamellar fashion, with the parallel fracture surfaces being at angles around 20 degrees to the longitudinal axis.
3. The compressive strength of the reinforced stubs was:
   218.3 kips with 4-#3 bars or 1.227% steel
   249.4 kips with 4-#4 bars or 2.182% steel
   compared to 269.6 kips for the unreinforced stub, a decrease of 18.8% and 7.5%, respectively. Failure was normally precipitated by the complete shedding of the concrete cover outside the bright wire spiral, upon which the remaining core became unstable and the test had to be discontinued.

   A close inspection of the fracture surfaces of the plain concrete stubs revealed no marks, which would normally identify action by shear friction; the surfaces had the exact appearance of those resulting from pure tension. Since no tensile stress can occur in a uniformly loaded column made of homogeneous material, the tensile fracture that

seems to develop must be caused by some interplay between a relatively small compressive stress, normal to the fracture surface, and the dominant shear stress, parallel to it. It now seems possible to formulate a new compressive fracture theory based on these observations, independent of Mohr's theory relative to principal stresses.

In view of it being in the domain of materials, any investigation thereof is clearly beyond the scope of this project. However, if it is true that, for whatever reason, significant tensile stresses develop in axially-loaded specimens nearly perpendicular (70°) to the direction of compressive stresses, a number of phenomena in the inelastic behavior of structural concrete may readily be explained.

4. Figure 6 illustrates a comparison of the standard 6x12-in. Standard American cylinder, the 8-in. cube used by some European countries, and the FDOT (which constitutes no standards whatsoever) column stubs. If 20° is taken as the approximate natural fracture angle, then the FDOT stub is the only one that will permit development of such fracture, without restriction normally present due to friction between the specimen and the platens of the testing machine. The compressive strength measured on the stub is more relevant to prismatic concrete components than either the cylinder or the cube. The cylinder test delivers an apparent strength of about 5% (4.5%), and the cube test about 30%, higher than the stub test. The restriction for the cylinder is small, but for the cube it is significant and, therefore, most European countries have already abandoned it. Either a 5x15- or a 4x12-in. test cylinder would better accommodate the 20° angle, although the latter may not be adequate for large aggregates.

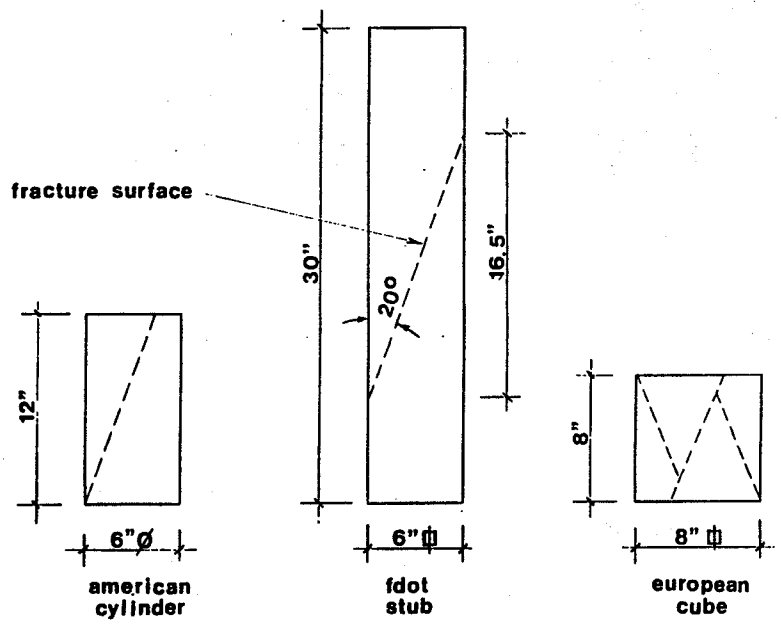

FIGURE 6 Comparison of compressive test specimens.

5. The presence of nearly lateral net tensile stresses at fracture provides a plausible explanation for spalling of the concrete cover. Figure 7 illustrates the vertical section of the round column and the horizontal section of a rectangular column. It is obvious that the steel cage creates a plane of weakness, exacerbated if the steel is epoxy coated, causing the cover to separate. The actual mechanics of effective core confinement appears to be one of arching between adjacent spirals or vertical bars, as the case may be, exerting an enhanced pressure thereon, especially on the corner bars, contributing to their buckling. It is also easy to see that if corrosion protection is obtained by increase of cover, the effectively confined core will be rather small, leading to potential structural instability.

6. It is often observed in testing concrete beams that the concrete top flange does not get crushed as expected, but fractures along a shallow diagonal line as indicated in Figure 8. Both the 20° and 45° angles are, of course, average values of large variations due to the complex stress distribution adjacent to the loading pad. Under and in the immediate vicinity of the pad, the vertical load causes a biaxial stress condition which prevents tensile fracture. This

phenomenon can be taken as an important linkage between prestressed concrete beams and columns, and will constitute one of the basic arguments in favor of treating them similarly in future bridge designs.

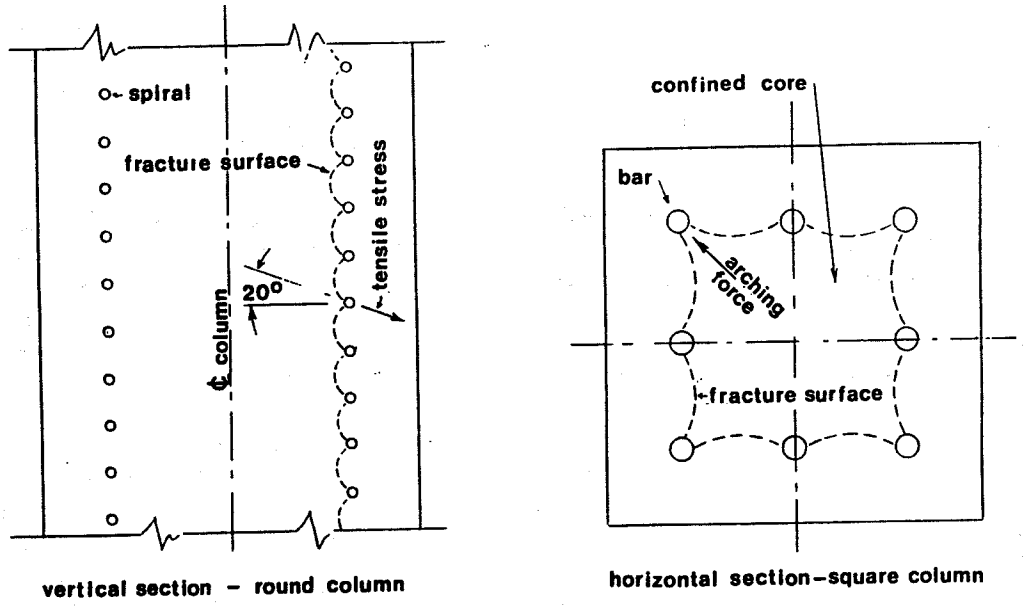

FIGURE 7 Observed spalling of concrete covers.

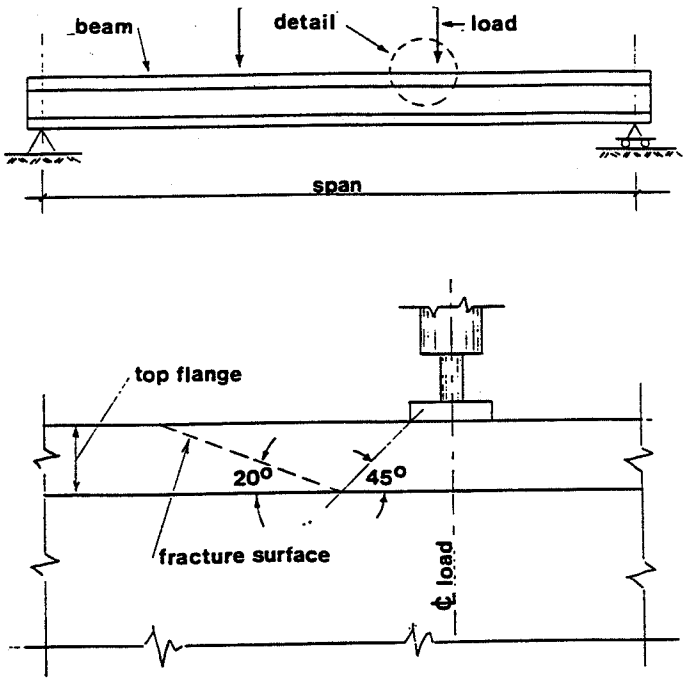

FIGURE 8 Compressive failure of top flange of beam.

INTRODUCING THE CPUC COMPONENT

The problems associated with reinforced concrete columns have been identified by several investigators in the past. The tendency of ties bending outward, the arching action between steel bars, and the reduction in the effectively confined sectional area, leading to reduction in strength and ductility, was identified by Sheik and Uzumeri (1980), Mander, Priestley, and Park (1988), and Cusson and Paultre (1994). Razvi and Saatcioglu (1994) state that effective confinement can be improved by closer ties, but this increases the susceptibility of cover separation. Inchionose (1995) claims that reversed cyclic loading often causes splitting bond failure in reinforced concrete columns.

On the other hand, Zia and Moreadith (1966) concluded that prestressed columns and piles, especially those subjected to large load eccentricity, offer high strength and ductility. Elias and Durrani (1988) and Carinci and Halvorsen (1987) reported that lateral reinforcement does not have any effect on the load carrying capacity of prestressed columns, and recommended elimination of the 0.85 strength reduction factor, since the concrete in such columns without ties is able to reach its theoretical ultimate strength value. One cumulative argument that can be derived from these studies is that the good performance of prestressed concrete columns is <u>not</u> conditional upon the presence of ties.

In fact, as the prestressing strands are in a state of high axial tension (approximately 6,000 microstrain), there is no possibility of premature strand buckling as the concrete approaches failure (approximately 3,600 microstrain). However, the elimination of ties or spirals does not resolve the corrosion problem of the strands. The first innovative idea of this project is the relocation of all prestressing strands into a central location by which the concrete cover is increased to the possible maximum. Typical cross sections of the centrally prestressed unreinforced concrete (CPUC) piles and columns are displayed in Figure 9. For the same level of prestress, the strands of the traditional pile design are simply moved into a central 2.0-in. grid pattern, similar to beams, and without ties. In the CPUC column, the strands are banded into a post-tensioning tendon, located in a central duct. The tendon can be loop-anchored in the substructure and the post-tensioning is carried out from the top of the superstructure, thus connecting the three components together.

The first reaction of nearly everyone who had been made acquainted with the CPUC idea, was the fear of losing flexural resistance. As illustrated in Figure 10, this is not the case. In the traditional layout, strands only in lines *b* and *c* can reach yield point, while the stresses in strands along line *a* are barely above the prestress due to their closeness to the neutral axis. In the CPUC layout, all of the eight strands attain the yield level, and although the internal moment arm for the yielded strands decreases, the ultimate CPUC flexural resistance of 2,795 k.in. exceeds that of the traditional pile with 2,720 k.in. The above values are based on the rectangular Whitney stress block as being slim first approximations.

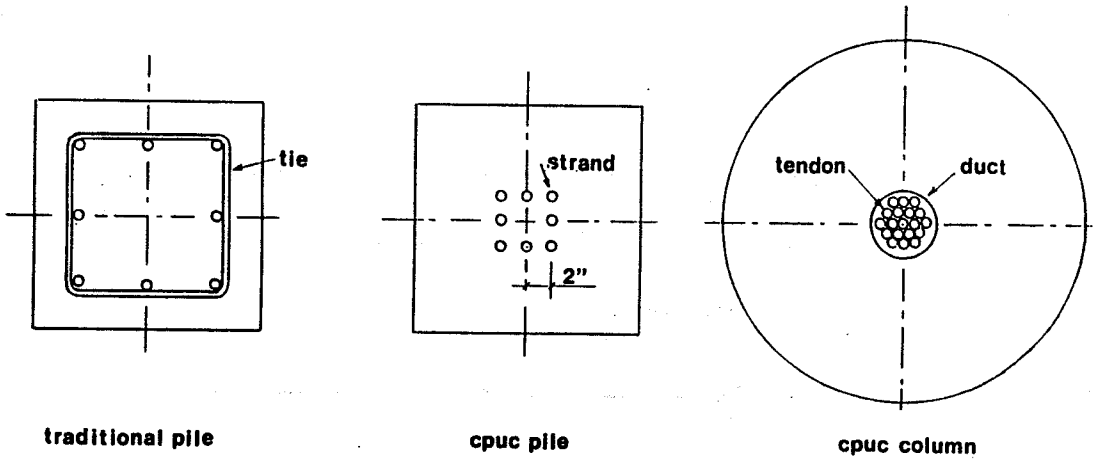

FIGURE 9 Traditional and proposed cross sections.

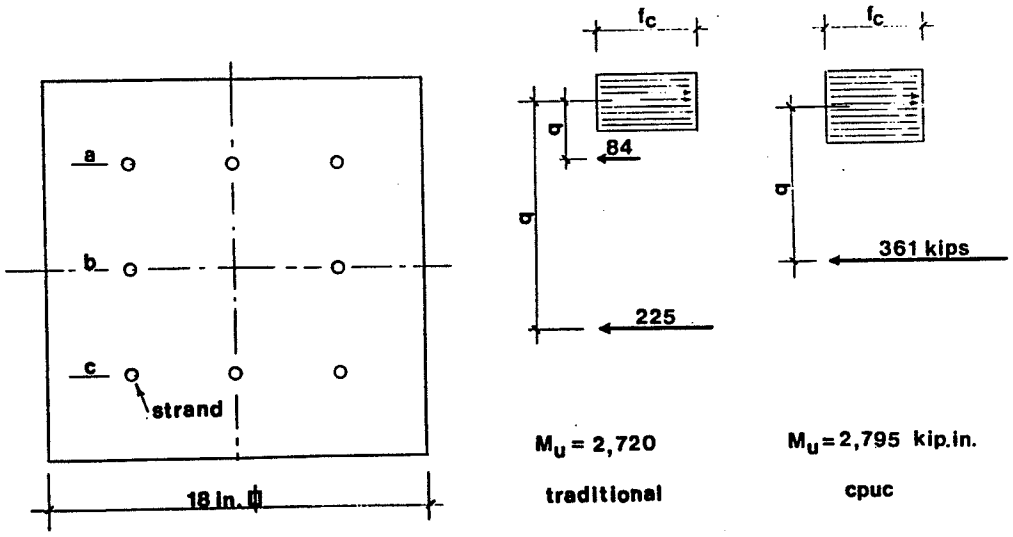

FIGURE 10 Comparison of flexural resistance.

INELASTIC ANALYSIS OF CPUC COLUMNS

In reality, the purely axial loading on columns and piles is physically impossible, therefore, they must be analyzed for combinations of axial load and moment. The inelastic analysis of the performance of eccentrically-loaded columns is rather difficult for a variety of reasons. For every increment in the concrete strain, a change will take place in the:

a. distribution of compressive stresses,
b. position of the neutral axis,
c. shape of the compressive area of the cross section for circular columns and for biaxial flexure of rectangular columns, and
d. elastic-inelastic strain distribution in the steel.

The LRFD Code specifies that the resistance of concrete components shall be based on the conditions of force equilibrium and strain compatibility, with the strain being directly proportional to the distance from the neutral axis. The concrete compressive stress-strain distribution may be assumed to be rectangular, parabolic, or in any other shape which results in a prediction of strength in substantial agreement with test results. One such "other" shape is represented by an exponential function, which was first developed by Smith and Young (1956). Unfortunately, the numerical process they promoted was so cumbersome and inaccurate that the exponential stress-strain relationship was not accepted for engineering applications in spite of the fact that it seems to offer the best correlation with test results.

The exponential relationship has recently been reviewed and found to be eminently suitable for the inelastic analysis of eccentrically-loaded columns and piles. The basic independent variable of this numerical system is the ratio α between the actual concrete strain ϵ and the strain ϵ_c associated with f_c', ($\alpha=\epsilon \div \epsilon_c$). As illustrated in Figure 11, α uniquely defines the distribution of compressive stresses. It can be seen that at $\alpha=0.2$, the distribution is virtually linear, at $\alpha=0.6$, inelastic behavior begins to show, and at $\alpha=1.0$, inelastic distribution prevails. The curve at $\alpha=1.4$ is what can be obtained by careful and precise compressive testing of short prismatic concrete specimens; it normally signifies the extent of their strain capacity. For medium strength concretes, the Hognestad limit approximates $\alpha=1.25$. Figure 11 also explains how the curves develop.

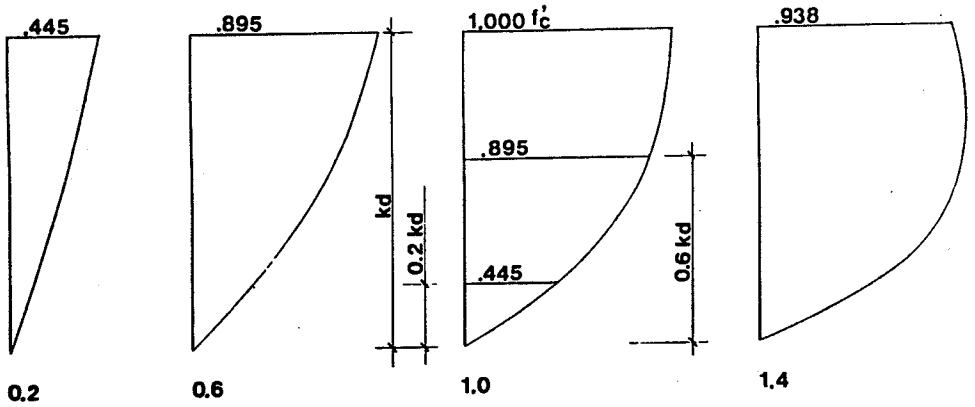

FIGURE 11 Distribution of compressive stresses as a function of α.

For introduction, an 18-in. CPUC pile will be analyzed. For rectangular cross sections in uniaxial flexure, the exponential function provides close form solutions for the compressive force N_c and its first moment M_c relative to the neutral axis. The CPUC column simplifies the calculations as the steel can be assumed to be bundled at its center. Figure 12 illustrates the unfactored axial load-moment interaction curve for an 18.0-in. square pile of 6,000-psi concrete with eight 0.5-in.-diameter, 270 ksi strands. The curve is discontinued at an eccentricity of 2.0 in., as the authors tend to believe that the minimum design offset should be the larger of 2.0 in. and one-tenth of the outside dimension of the pile (1.8 in. here) or column. At cutoff, the ultimate axial load and moment are 1,330 kips and 2,665 k.in., respectively. The maximum moment resistance is 4,155 k.in., which is mobilized at an axial load of about 750 kips. According to oral communication from FDOT, the maximum design capacity, as determined by soil conditions, never exceeded 600 kips.

The interaction diagram indicates the point where the steel changes from being elastic to inelastic. It should be noted, however, that the steel is inelastic below the yield point, and as the load increases, the steel stress decreases. When $\Re$=1.0, the stress is the prestress, and it is at a minimum when the axial load is at a maximum. Accordingly, the conditions developing at the strength limit states are entirely different from those codified for the design of prestressed concrete beams, and should, therefore, not be applied.

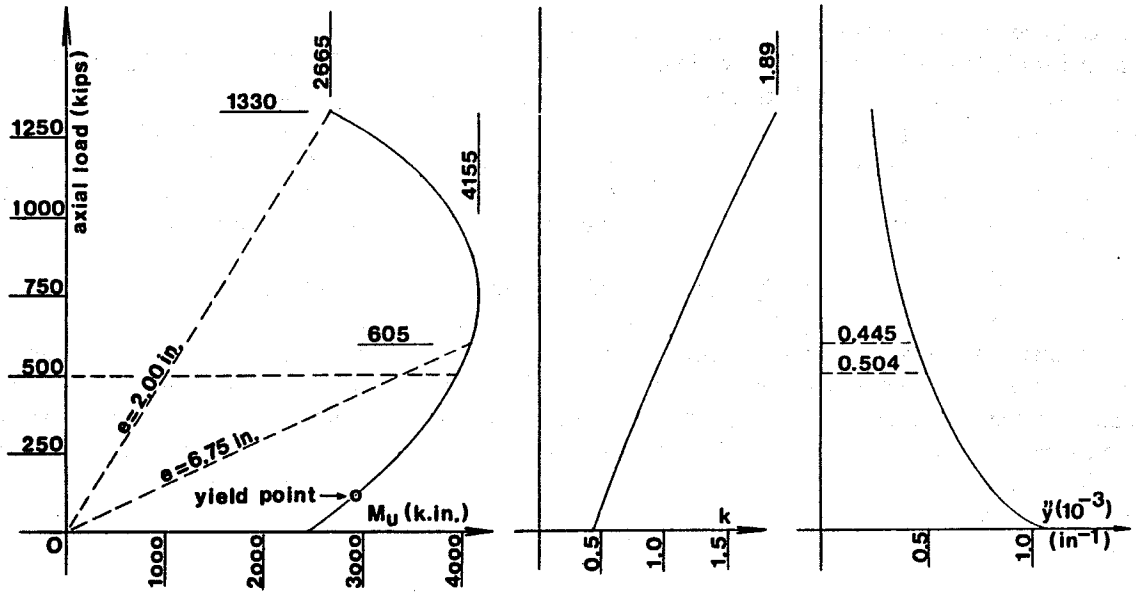

FIGURE 12 Interaction diagram for 18in. square pile.

Also shown in Figure 12 is the $\Re$ diagram (such that $\Re d$ is the depth of the compressive stress diagram). From 0.479 at zero axial load, it increases in a nearly linear fashion to 1.89 at the cut-off point. It may be noted that the cross section would be fully in a state of compression at $\Re$=2.0 in. Indicated on the right-hand side is the second derivative (γ'') of a deflection curve, which is also the rotation of the column per unit length, and the inverse of which is the radius, $\Re$, of curvature. At Q=500 kips, $\Re$=1 ÷ 0.504 x 10^{-3}= 1,984 in. If the free length of the column is 16.0 ft., the central deflection can be calculated as 2.32 inches, and with 40.0 ft., as 14.51 inches. These figures indicate high level flexibility, and the fact that P/Δ effects cannot be avoided at the strength limit states.

The performance of a cross section between zero and ultimate loads can be demonstrated by taking either the axial load or the eccentricity constant. Figure 13 demonstrates the development of moments for zero and 500-kip axial loads as functions of α for both the CPUC and the traditional designs. It can be seen that for pure flexure (Q=0), the traditional design produces slightly higher moment than the CPUC at the beginning; but at ultimate, the CPUC takes over. For Q=500 kips, the CPUC is marginally lower than the traditional design for the whole valid strain spectrum.

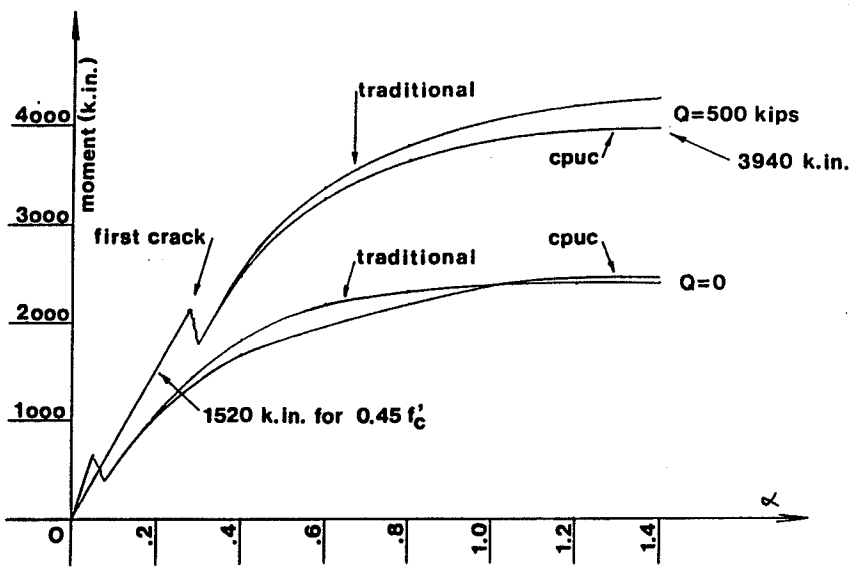

FIGURE 13 Moments for constant axial force.

A number of other observations could also be made in general for prestressed columns. Under axial load, the curve continues to rise to the ultimate; a flat plateau would be undesirable for flexible columns relative to P/Δ effects.

The moment for 0.45 f_c' at the service limit state is 1,520 k.in. The resistance at the strength limit state is 3940 k.in., or 2.59 times the previous figure, which suggests that such a service limit state is unnecessary. This limit state is also not being associated with any benchmark on the curve. It is meaningless and should, therefore, be eliminated from the design of prestressed columns and piles.

Similar to that of any prestressed concrete component, the curve suddenly drops upon first cracking and then rebuilds itself as the strain increases. No matter what happens, the curve will never return to the initial cracking point, as the concrete has lost its tensile strength, and the resulting crack will open up at a lower load, which renders the first crack as a service limit state completely invalid and without a defensible objective. The CPUC column is not really susceptible to corrosion, yet uncontrolled crack openings may not be desirable. Since corrosion is a time-dependent action, the cracking limit state should be replaced by a crack-opening limit state for which only permanent force effects, but including those due to shrinkage, creep, and settlement, should be considered.

Figure 14 demonstrates the development of axial force as a function of α for an eccentricity of 6.75 in., which corresponds to 1.50-in. offset for the 4x4-in. specimens used in the column tests of this project. The curve is similar in

nature to those shown in Figure 13. Again, first cracking is immediately followed by inelastic action. Deformation of a 141.75-in.-long column, which corresponds to the tested specimens, yields a transverse deformation of 1.09 in., increasing the maximum eccentricity to 7.84 in. This intercepts the interaction curve at a lower point. The maximum deformation y_0' can be calculated from:

$$48\Re y_0^2 + [48\Re \iota - 5\iota^2] F_0 - 6\iota e = 0$$

where:

$\Re$ = radius of curvature $(1 \div \gamma'')$
e = initial eccentricity
ι = length of hinged column

As e is not constant, the actual y_0 can only be obtained by successive approximation. In this case, the final values are:

y_0 = 1.25 in.
Q = 490 kips
M = 3,920 k.in.
$\Re$ = 1,960 in.

This calculation indicates that the investigation for P/Δ effects in the inelastic phase can be reduced to simple geometrical manipulations.

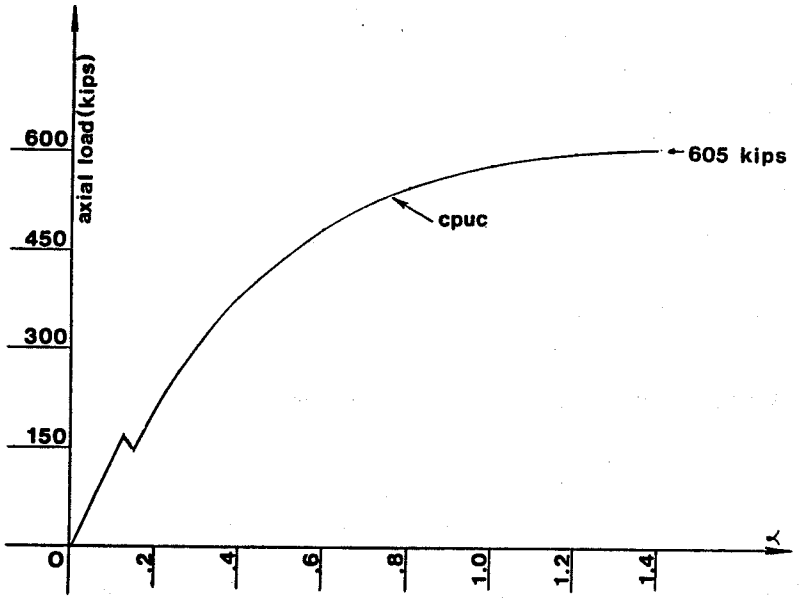

FIGURE 14 Axial load for an eccentricity of 6.75 in.

EARTHQUAKE APPLICATION OF CPUC COLUMNS

As shown above, the CPUC columns are expected to perform well in terms of flexibility and ductility, and have the potential of being used everywhere in the United States except in areas of high seismicity. Although the CPUC is more flexible than the normally reinforced column, it still is unable to match flexibility and strength requirements in these areas. The problem at the core is the low-strain capacity of unconfined concrete, as we know it.

The general lack of flexibility of concrete structures had been noticed early in this century. Freyssinet, first recognizing the plastic capability of concrete necks, designed an inelastic hinge, consisting of a narrow concrete strip of low depth, which derives both its strength and flexibility from being confined by the two structural components it

connects, and from lateral shear friction. The Freyssinet hinge became quite popular in Europe during World War II for application in large rigid frames of industrial buildings.

Cuzens (1954) carried out a large number of prototype tests by which the design characteristics of the hinge had been established. The only well-known application of the hinge in the U.S. is in the V-piers of the Long Key Bridge in Florida. For perceived safety reasons, however, the designer placed vertical high strength steel bars at the center line of the hinge, thus turning the hinge into a miniature reinforced concrete component by which its innate ability of accommodating concentrated rotations had to be bifurcated, resulting in excessive cracking.

The second innovative idea in this project is the recognition of combining the CPUC column, having all its steel centrally located, with an inelastic device with extended flexural capability. If founded on the Freyssinet Principle, such a device has to satisfy the following conditions:

a. in order to prevent load sharing between the steel and the concrete in the device, the steel should be unbonded;
b. the steel should be made free to accommodate the concentrated rotation taking place in the device;
c. the device should be multidirectional to be able to resist earthquake action in any lateral direction; and
d. in order to permit extremely high (50,000 psi) stresses, the concrete in the hinge should be confined both internally and externally.

Figure 15 illustrates both the Freyssinet hinge as embellished for the Long Key Bridge application, and the current innovation labeled as the Extended Performance Flexural (EPF) device. The EPF device replaces the modified Freyssinet hinge, detailed in the Annual Progress Report (December 1992) of NCHRP-IDEA, as the latter was not found to be feasible.

The EPF is not an isolator, but a completely structural device intended for connecting pier columns to either the superstructure or the substructure, or both, and transmitting considerable moments while permitting large rotations. As indicated in Figure 15, it consists of:

a. two concentric confinement rings which do not participate in resisting axial stresses;
b. a doughnut-shaped concrete wafer located between the confinement rings;
c. two compressive rings, acting both as pistons and bearing plates, which transmit compression between the wafer and the structural concrete; and
d. a metal band (not shown), an accessory to the device, to prevent tensile splitting of an unreinforced column.

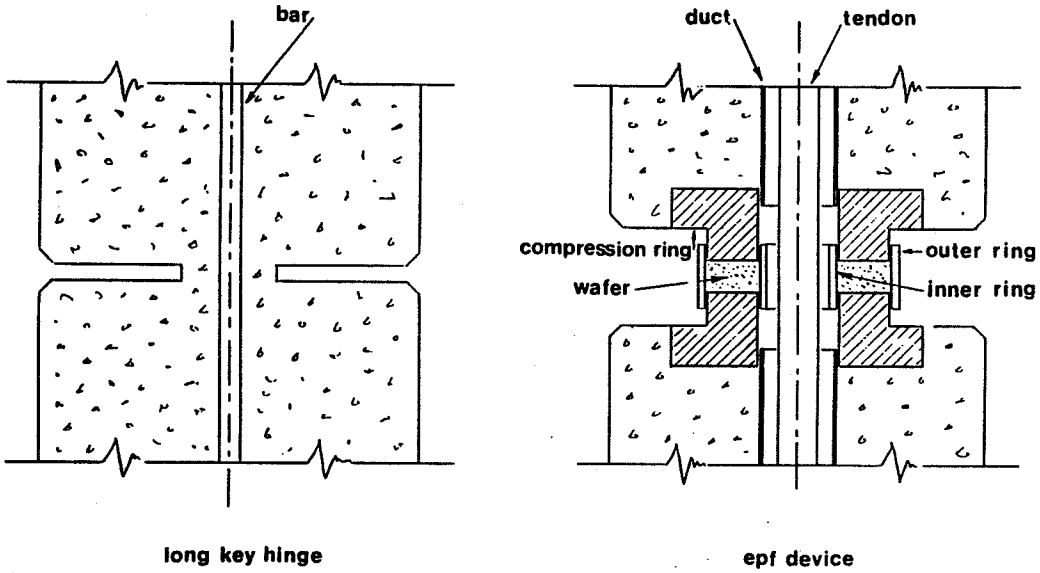

FIGURE 15 Inelastic concrete rotational devices.

There is play between the piston part of the compression ring and the confinement rings to permit rotation of the device. Nearly the entire rotation emanates from the compressibility of the wafer. The prestressing tendon is free at and in the vicinity of the device, it is anchored in both the substructure (by loop) and the superstructure (by mechanical means), and may be partially grouted in the column. Away from the device, the tendon is housed in heavy-duty ducts. The wafer itself can be tailored to meet specific needs. The thinner the wafer, the higher is its resistance to compressive stresses. It may be precompressed to minimize initial deformations. The aggregate in the wafer may range from ordinary lime rock to silicon carbide which is the hardest material after diamond.

COMPRESSIVE TESTS

SHORT COLUMN TESTS (SERIES A)

In the preliminary FDOT tests, the compressive failure of prismatic concrete specimens appeared to be tensile in nature. It had also been observed that the inclination of the lamellar fracture surfaces to the longitudinal axis of the specimens tested with remarkable consistency at about 20°. Since the development of tensile stresses cannot be explained by the Principal Stress Theory for homogeneous materials, it was necessary to confirm these preliminary observations on a broad basis, as they seemed to contain the seeds of plausible explanations for the failure modes of structural concrete components.

Series A was planned to test 48 unreinforced concrete specimens in compression, including four concretes in four different shapes in order to study the:

a. mode of compressive failure,
b. effect of compressive strength on the failure mode,
c. effect of shape on the compressive strength, and
d. effect of size on the compressive strength.

Designated concrete strengths were 3,500; 5,000; 6,500; and 8,000 psi. The specimens were 6" x 12" standard, 4"x 8" and 4"x12" cylinders, and 4"x 4"x12" square prism stubs. The concrete mix design details were obtained from the Florida DOT Material Testing Laboratory, Gainesville, Florida. The following materials were used in the concretes:

Coarse aggregate:	3/4" Florida lime rock
Fine aggregate:	Screening
Cement:	Type II
Flyash:	Class F
Air entrainer:	Darex aea - W. R. Grace & Co.
Water reducing admixture:	WRDA79 - W. R. Grace & Co.

The actual mix designs per cubic feet of concrete are given in Table 1.

TABLE 1 Concrete Mixture Design

Material	Specified 28-day compressive strength			
	3,500 psi	5,000 psi	6,500 psi	8,000 psi
Cement	13.5 lb	17.8 lb	2.12 lb	23.6 lb
Flyash	3.5 lb	4.5 lb	5.3 lb	5.9 lb
Coarse Aggregate	63.4 lb	61.5 lb	62.9 lb	65.3 lb
Fine Aggregate	50.3 lb	47.4 lb	41.4 lb	37.2 lb
Water	9.5 lb	10.5 lb	10.4 lb	10.2 lb
Air Entrainer	0.2 oz	0.2 oz	0.4 oz	0.5 oz
Admixture	1.3 oz	1.3 oz	1.8 oz	2.1 oz

The specimens were tested at or about 28 days. With the exception of the 8,000-psi designation, all the concretes generally exceeded the designated strength. A closer examination of the 8,000-psi specimen results revealed no statistically identifiable difference between the 6,500-psi and 8,000-psi concretes. There are two plausible explanations for this. As shown in Table 1, the difference in the mixture design between these two concretes is very small; therefore, the probability exists that the 6,500-psi mixture was accidentally used for both. The other explanation is that the strength of these concretes may be limited by the coarse aggregate, particular to Florida, which is not a limestone, but an unconsolidated limerock of a porosity that provides for excellent adhesion with the cement matrix, but with limited strength.

The loss of the 8,000-psi concrete specimens is unfortunate but not significant. By lumping the two concretes together, the number of specimens for the 6,500-psi concrete is actually doubled to a level of statistical significance. The test results and the computation for mean, standard deviation (Std.D), and the coefficient of variation (C.V.) are shown in Table 2.

TABLE 2 Test Results for 6,500-psi Concrete Specimens (Strength in Psi)

	6"x12" cylinder		4"x8" cylinder		4"x12" cylinder		4"x4"x12"stub	
Sl. no.	f'_c	$(\Delta f)^2$	f'_c	$(\Delta f)^2$	f'_c	$(\Delta f)^2$	f'_c	$(\Delta f)^2$
1	7428	7921	6165	156816	7165	841	6504	544644
2	7641	15376	6585	576	7367	53361	7472	52900
3	7747	52900	7006	198025	7379	59049	7935	94249
4	7640	15129	5704	734449	6904	53824	8168	857476
5	7216	90601	7347	617796	7045	8281	6909	110889
6	7428	7921	----	----	6956	32400	7462	48400
Total	45100	189848	32807	1707662	42816	207756	43450	1708558
Mean	7517		6561		7136		7242	
Std.D.		194.85		653.39		203.84		584.56
C.V.		2.59%		9.97%		2.86%		8.07%

The 6"x 12" standard cylinders were tested in a universal testing machine with the platens fitted out with confined neoprene pads, requiring no capping of the specimens, at the PSI Testing Laboratory, West Palm Beach, Florida. The pads are believed to provide excellent uniformity of compressive stress distribution by reducing lateral stresses that develop due to friction at the interface between the specimen and platens. The pads, because of their different color, facilitate the central positioning of the specimens in the machine. The favorable expectations were borne out by the test results, with the average strength of 7,517 psi being 15.6% above the designated strength, and with the coefficient of variation as low as 2.59%.

The 4"x 8" and 4"x 12" cylinders were tested in a more traditional compression testing machine requiring capping of the specimens. There is no plausible explanation for the 4"x 12" cylinders having a compressive strength higher than the 4"x8" cylinders, as shown in Table 2, other than the possibility that the former were positioned in the testing machine with more care relative to centrality. On the basis of the comparatively high average strength of 7,136 psi, 9.8% above designated strength, and the low 2.86% coefficient of variation, the 4"x 12" cylinder was employed as the control specimen for all further testing.

The 4"x 4"x 12" stubs were tested in another machine, more suitable for specimens with rectangular footprints. Instead of capping, these specimens were cast against 4"x 4"x 1.25" steel end plates which were secured to the concrete by taping. The 7,242-psi average compressive strength, 11.4% above the designated value with an 8.07% coefficient of variation, normal for the given strength level, was taken as indicative of the accuracy expected from small scale models.

Table 3 is a summary of the compressive test results for 5,000- and 3,500-psi designations. Both concretes indicate excellent consistency of the 6"x 12" cylinders tested with neoprene pads. The average strengths of both concretes in 4"x 4"x 12" stub testing slightly exceeded their 6"x 12" cylinder strength, a reversal of the 6,500-psi concrete results; the variation among individual specimens was high. For both concretes, the 4"x 8" cylinders showed marginally higher strength than the 4"x 12" cylinders; this also represents a reversal of the 6,500-psi concrete results.

TABLE 3a Results for 5,000-psi Concrete Specimens (Strength in Psi)

Sl. no.	6x12 in. Cylinder	4x8 in. Cylinder	4x12 in. Cylinder	4x4x12 in. Cylinder
1	6,367	5,967	6,433	7,010
2	6,367	6,091	6,173	6,834
3	6,579	---	5,306	5,997
Mean	6,438	6,029	5,971	6,614

TABLE 3b Results for 3,500-psi Concrete Specimens (Strength in Psi)

Sl. no.	6x12 in. Cylinder	4x8 in. Cylinder	4x12 in. Cylinder	4x4x12 in. Cylinder
1	5,182	4,936	4,665	4,900
2	5,235	4,773	4,442	5,029
3	5,041	----	----	5,895
Mean	5,153	4,854	4,553	5,275

Based on the weighted averages for all the test specimens considered, the ratios of the strengths to those obtained for the standard 6"x 12" cylinder were as follows:

4"x 8" cylinders: 0.902
4"x 12" cylinders: 0.927
4"x 4"x12" stub: 0.994
All cylinders: 0.916

There were no discernible indications of size effect.

The failure modes were carefully recorded for the 44 tests that were actually performed (four of the total of 48 cast were lost due to various reasons). In 37 cases, the inclined fracture surfaces could clearly be identified. They were best demonstrated by the slender 4"x 12" cylinders, probably because in these cases, the fracture mechanisms were least disturbed by interface confinement due to the platens. In many cylindrical specimens, the slanted fracture surfaces took helical shapes, leaving largely intact cones at the ends. The actual fracture angles were not measured, but estimated and recorded. There appears to be a slight inverse relationship between the compressive strength and the angle of fracture. For the lower strengths, the angle approximated to 20°. For the higher strengths, angles as low as approximately 15° were recorded. The fracture surfaces were examined and without exception, the surface cut through the coarse aggregates and appeared to result from pure tension.

Some of the failure patterns are shown in Figure 16. In all cases, the failure was massive, with tensile fracture taking place at a multiple of planes. The remaining seven specimens failed in various ways, such as complete granulation of the concrete, vertical splitting, and/or localized crushing. It can be concluded, therefore, that:

1. the compressive failure of concrete can more precisely be diagnosed as a consequence of one mode of tensile fracture;
2. for the range of concretes tested, the angle of fracture to the longitudinal axis of prismatic components is between 15° and 20°;
3. in reinforced concrete columns, the tensile stress at fracture is nearly perpendicular to the steel cage, by which spalling of the concrete cover under axial compression is accelerated;
4. improvement in (apparent) compressive strength can only be attained by decreasing or eliminating the tensile stress by either passive or active confinement;
5. slender test specimens which permit the 15° and 20° unrestricted fracture planes are likely to give more realistic f_c' values for design; and

6. f_c' values obtained by the standard cylinders may need to be reduced by a multiplication factor of 0.90 to 0.95, but not the 0.85 value currently used.

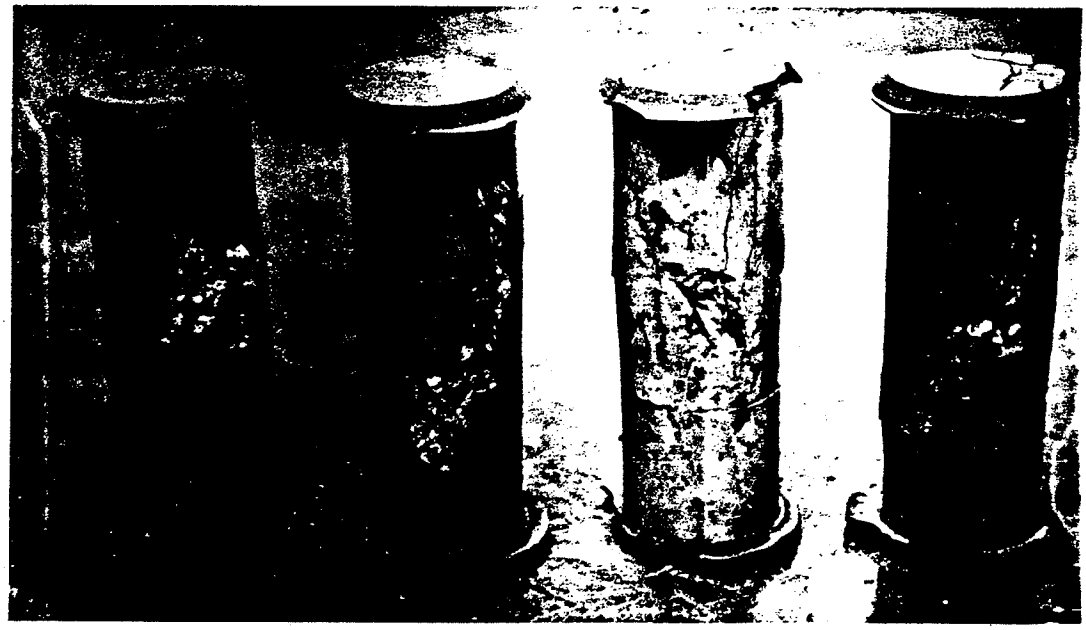

FIGURE 16 Photograph of failure patterns.

COLUMN TESTS (SERIES B, C, D AND E)

In order to compare the performance of the CPUC design with that of reinforced columns and traditionally prestressed components, a total of 16 valid compression tests were carried out. All test specimens were 4"x 4"x 29" stubs of nominal 5,000-psi concrete whose mix design is given in Section 3.1. The specimens were cast against 4"x 4"x 1.25" steel end plates for better fit. As illustrated in Figure 17, the steel plates were countersunk to accommodate a 1.0-in.-diameter hard steel ball by which eccentricity of the load was controlled. Center-to-center distance of the balls was 32.0 in., providing an l/r ratio of 27.7.

Figure 17 is a synopsis of test specimens and testing hardware, and it should be read in conjunction with Table 4. The second column in Figure 17 indicates the test setup, while the first one shows details of the bearing plates which, in addition to the countersunk ball-nests, include holes for the prestressing wires. The third column shows details of three columns with variable longitudinal reinforcement and constant spirals (0.125"-dia. wire, 0.5-in. pitch). In the fourth column, the top cross section represents the traditional arrangement of prestressing strands, while the central and bottom cross sections illustrate the CPUC design, with 0.75-ksi and 1.50-ksi prestress, respectively. In order to permit direct comparison between traditional and CPUC designs, the transverse reinforcement was omitted from the former. It should be noted that the CPUC design requires no transverse reinforcement, but accepts it if so desired.

For making the test specimens, two demountable and reusable formwork assemblies were built, consisting of layers of high-grade plywood, glued together and sealed against water intrusion. During construction, the elements of the forms were simply clamped, which permitted easy removal of the specimens and cleaning of the form surfaces. The formwork was designed to resist an axial prestressing force of 24.0 kips when clamped together. For prestressing, the ends were fitted out with double-decker steel devices, which allowed both prestressing and anchoring operations. The assembled prestressing unit with formwork is shown in Figure 18. The end unit configurations, stressing and fixed, are shown in

TABLE 4 Column Test Results (Series B, C, D, and E)

TEST	TYPE	STEEL	PRESTRESS (KSI)	ECCENTRICITY (IN.)	TRANSVERSE STEEL	FAILURE MODE	FAILURE LOAD (KIPS)
C1	Plain	None	None	0.00	None	Crushing at Mid Point	97.9
C2	Plain	None	None	0.75	None	Inclined Failure Plane	64.1
C3	Plain	None	None	1.50	None	Inclined Failure Plane	21.0
B1	Traditional	4-#3 Bars (2.76%)	None	0.00	Spiral	Partial Vertical Split	91.5
B2	Traditional	8-#3 Bars (5.52%)	None	0.00	Spiral	Unidentified	110.6
B3	Traditional	12-#3 Bars (8.28%)	None	0.00	Spiral	Unidentified	124.2
B4	Traditional	4-0.167" ϕ Wires	0.75	0.00	None	End Crushing	90.1
B5	Traditional	4-0.167" ϕ Wires	0.75	0.75	None	Compressive Crushing	56.6
B6	Traditional	4-0.167" ϕ Wires	0.75	1.50	None	Compressive Crushing	24.5
D1	CPUC	4-0.167" ϕ Wires	0.75	0.00	None	Compr. Failure at Center	110.6
D2	CPUC	4-0.167" ϕ Wires	0.75	0.75	None	End Crushing	65.9
D3	CPUC	4-0.167" ϕ Wires	0.75	1.50	None	End Crushing	27.4 x
D4	CPUC	4-0.167" ϕ Wires	0.75	±1.50	None	Crushing at En d Plate	41.4
E1	CPUC	6-0.167" ϕ Wires	1.50	0.00	None	Crushing at Center	87.2
E2	CPUC	6-0.167" ϕ Wires	1.50	0.75	None	Inclined Failure at Center	53.9
E3	CPUC	6-0.167" ϕ Wires	1.50	1.50	None	Crushing at End Plate	26.2

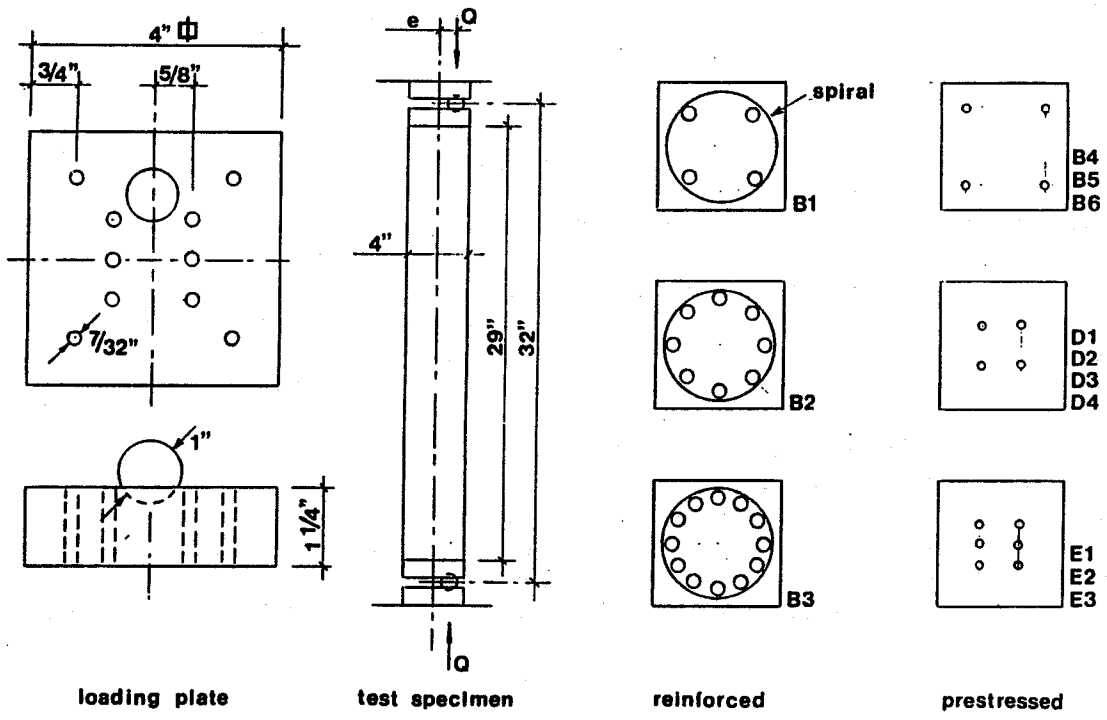

FIGURE 17 Synopsis of test specimens and hardware.

FIGURE 18 Assembled prestressing unit with formwork.

Figure 19. Each of the 96.0-in.-long formwork assemblies enabled the casting of three specimens at one time. The specimens were cast in a horizontal position. Getting the concrete inside the reinforcing cage (B1, B2, and B3) was just as difficult as getting the concrete into the space between the formwork and the cage in prototype construction for producing honeycomb-free covers.

The first comparison can be made among the specimens C1, B1, B2, and B3, all tested with (near) zero eccentricity. Failure loads are given in Table 4, and the results illustrated on the left-hand side of Figure 20. They actually confirm the original FDOT tests values, shown on the right-hand side, in that the steel initially reduces axial resistance, and that it takes a considerable amount thereof to regain the loss. Examples of the failed columns are shown in Figures 21 and 22. Potential resistance lines, tied to the tested plain concrete column C1, indicate what might happen if the steel and concrete were structurally compatible at failure. Test results fall at about three quarters, and the LRFD-factored resistance at about one half, respectively, of the potential line. The low LRFD values are understood to cover unintended and uncontrollable small eccentricities. The designer cannot improve upon the performance of reinforced columns, as no accepted model exists, by which the interaction between the steel and concrete in the inelastic phase could adequately be described.

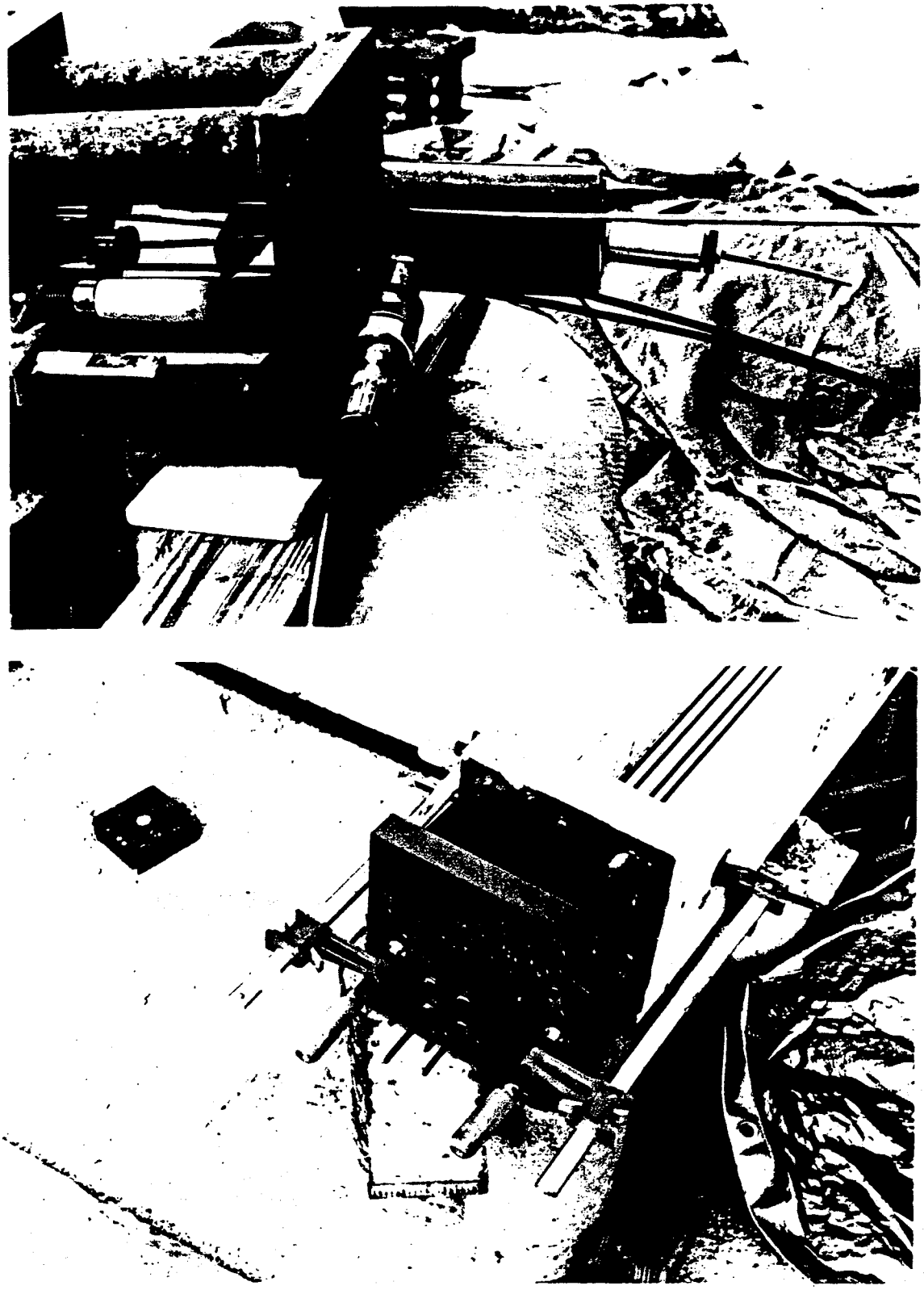

FIGURE 19 ***Top:*** **The stressing end.**
Bottom: **The fixed end.**

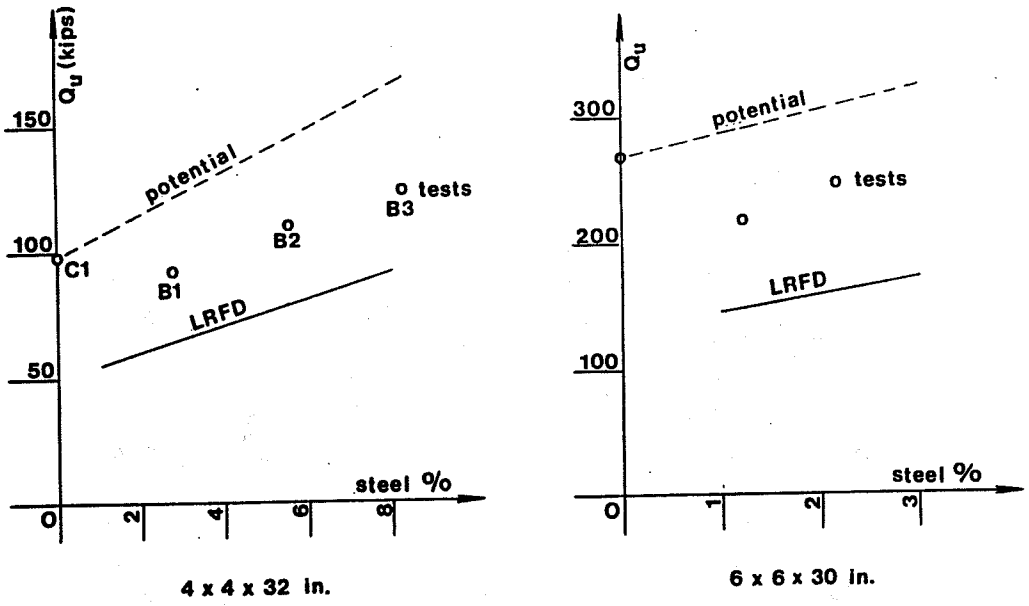

FIGURE 20 Performance of reinforced columns.

Figure 23 illustrates the force-deflection diagram obtained from the CPUC specimen D3. It failed at a load of 27.4 kips, acting with an eccentricity of 1.50 in. D3 can be considered as a 1:4.5 scale model of the 18-in. pile investigated in *Inelastic Analysis of CPUC Columns*, yielding a strength of 490 kips at a deflection of 1.25 in. After adjusting for the difference in f_c' (6,690 vs. 6,000 psi) and applying scale factors, these translate, as shown in Figure 23, to 26.9 kips and 0.278 in. The specimen failed in two steps: The first crack occurred at a load of 19.2 kips, and there was no further visible action until failure, at which time a triangular piece, with side angles approximating 20° to the center line, broke out of the specimen. This mode of failure is similar to that for prestressed concrete beams. This, and the good correlation between predicted and tested values, indicate that, in terms of reliability and thus resistance factors, the CPUC column may be treated at ultimate limit state as a prestressed concrete beam.

For components in which the steel does not yield at failure, it is customary to define ductility as the ratio of the deformation at ultimate and the projected (virtual) elastic deformation. As shown in Figure 23, these values are 0.278 and 0.0618 in., respectively, producing an adequate ductility number of 4.5.

Due to time constraints, some of the column tests were carried out at ages different from 28 days. All control specimens were 4"x 12" cylinders. The 28-day strength of columns in Series E were obtained by extrapolation using test results of control specimens.

In Figure 24, comparisons are made between CPUC (D-Series) and traditionally prestressed columns (upper B-Series), and between CPUC columns with 0.75 ksi (D-Series) and 1.50 ksi (E-Series) prestress. The CPUC-D1 specimen with zero eccentricity carried a load of 110.6 kips, or f_c' = 6,812 psi, which is above the average for 4"x 12" cylinder tests of 6,690 psi. Even if D1 is discounted as an extreme, the CPUC curve is consistently higher than the traditional curve, faring better than expected by analysis. The resistance of the CPUC specimens with 0.75-ksi prestress was marginally higher than those with 1.50 ksi, except in the area of high eccentricity. This is quite natural as the part of the prestressing force that remains due to the axial load is from the compressive resistance of the concrete. With higher eccentricity, the flexural effects tend to dominate, and the higher flexural resistance reflects the influence of more steel being present. It is obvious that the level of prestressing in prototype construction should be kept to the minimum which satisfies flexural requirements.

It should be noted that for Figure 24, the E-Series values obtained at the age of 17 days, and given in Table 4, have been upgraded by the control cylinder strength ratio of 5,500 psi to 6,015 psi.

In summary, these tests indicate that the CPUC design:

a. when used in piles, is at least as good as the traditional design;
b. requires no transverse steel and a minimum (0.5% to 1.0%) amount of prestressing steel;
c. has adequate ductility;
d. fully utilizes the resistance of concrete; and
e. its resistance, including P/Δ effects, is predictable by analysis.

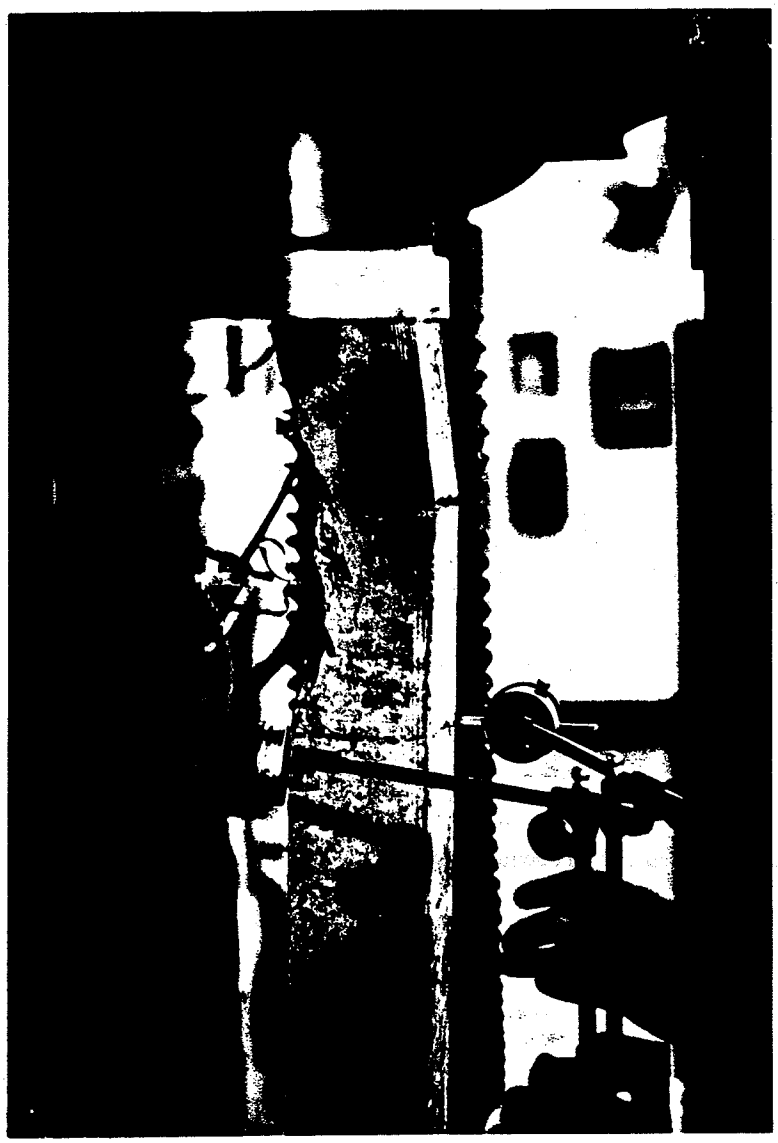

FIGURE 21 Example of a column after testing.

FIGURE 22 Failure pattern of a CPUC column (specimen D3, eccentricity=1.50 in).

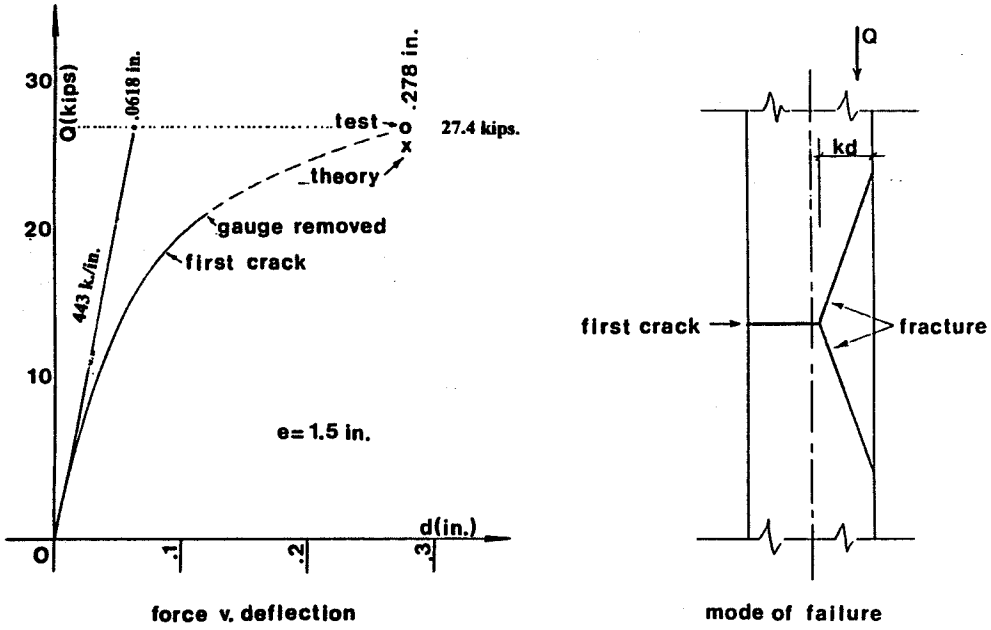

FIGURE 23 CPUC test D3.

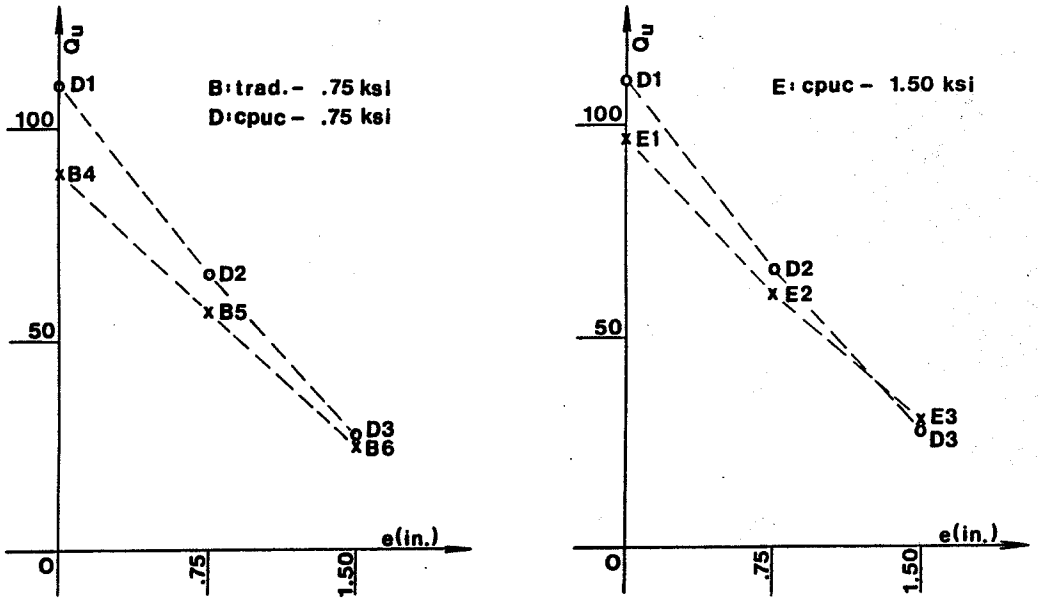

FIGURE 24 Comparison of axial resistance.

DEVICE FOR EARTHQUAKE RESISTANCE

FLEXURAL TESTS

The EPF device is described in *Earthquake Application of CPUC Columns*, and its details are displayed in Figure 15. The objective of this series of testing was to experimentally obtain the moment-rotation curves, which are characteristic for the EPF device as a function of the material and height of the cementitious wafer in the device. This was the only possible avenue to be taken since the device is operating at stresses and strain rates for which information is simply not available.

A pictorial schematic of the EPF testing apparatus, specifically designed and manufactured for this project, is illustrated in Figure 25. It consists of two reinforced concrete blocks, encapsulated in steel boxes fitted out with moment arms. The photographs in Figures 26a and 26b show a loading block before and after concreting. The blocks are nested to receive and to facilitate replacement of the EPF. The axial force is generated by a top-mounted 60-ton, double-acting jack via a 1.0"-diameter Dywidag bar which is located in 1.5"-diameter rigid ducts and anchored at the top and bottom. Figure 27 shows the threaded prestressing bar with the assembly. The moment is delivered by an offset mounted 5-ton double-acting jack. Deformations were measured by three dial gauges (the third one, located at the center line on the backside, is not shown). The jacks were operated by separate oil pumps. Figures 28 and 29 demonstrate the compression and tension modes.

The apparatus had two minor shortcomings which could not be overcome primarily due to budget limitations. One is that the reversible P-force is either additive or subtractive relative to the actual compressive force resisted by the EPF, although the variation did not exceed ±5.7 of the primary Q-force. The second is that the compressive force in a bridge is a sum of two components, namely the prestressing and the dead load reaction. The latter causes P/Δ effects which could not be simulated by this apparatus, nor by standard testing machines, had they been available.

The inside diameter of the outside confinement ring and the outside diameter of the inside ring were 3.068-in.and 1.900-in., respectively, providing a wafer area of 4.56 in.^{2} Details are shown in Figures 30a and 30b.

In the first step, the maximum uniform stress, as indicated in Figure 31, was caused by a central force of 86.2 kips. Figure 31 shows the normalized test results of three wafers, namely:

- 0.5-in.-deep 5,000 psi limerock concrete,
- 1.0-in.-deep coarse silicon carbide with 5% cement, and
- 0.5-in.-deep medium silica sand with 5% cement.

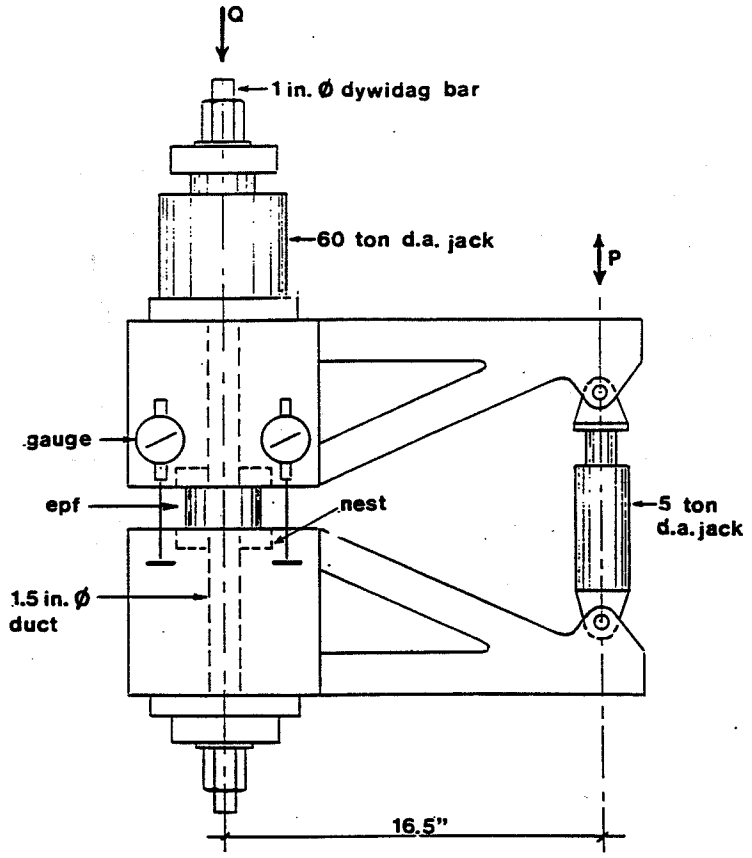

FIGURE 25 EPF testing apparatus.

Materials other than limerock were used to see the pulverizing effects of cyclic loading. Indeed, the concrete exhibited some pulverizing, the silica sand, little, and the carbide, none. The concrete alone shows a discontinuity in the stress-strain relationship: At a stress of about 9.5 ksi, the cement matrix is believed to disintegrate and, with all the internal voids filled, the rise in all the materials becomes similar. It should be noted that none of the curves demonstrate any sagging that characterizes the behavior of unconfined structural materials. It is obvious that by varying the composition of the wafer, in terms of both materials and gradation, various structural requirements can be met.

In the second step, each of six EPF devices was tested for three full cycles of eccentric loading by operating the 5-ton jack, while maintaining pressure on the central jack. The hydraulic system did not permit controlled unloading; therefore, the unloading segments of the hysteresis curves are estimated. The first cycle hysteresis curve of a 1.0-in. limerock concrete wafer is demonstrated in Figure 32. In both positive and negative rotation, the curve exhibits significant plasticity; the energy absorbed by the device is defined by the area within the curve, or about 3.9 kip. in.

Figure 33 indicates three consecutive half-rotation curves for a 0.5-in. silicon carbide wafer. The researchers were reluctant at first to extend the rotation range beyond the design limit of ±5.0% for fear of breaking the Dywidag bar. But, as the curves were still rising at that limit, the rotation was extended to twice that value. The cycling seems to stiffen the device, and to converge its responses; test (cycle) curve 3 is probably close to the final configuration. With respect to the concrete wafer (performance shown in Figure 32), both the moment and rotation ranges had been extended from 58.4 to 99.3 k.in. and 5.7% to 9.5%, respectively. A comparison of Figures 32 and 33 is also indicative of the influence the wafer depth plays in determining the response characteristics of the EPF device.

The overall test data, including results (A.1), cumulative rotations (A.2), and moment-rotation curves (A.3), are located in Appendix Section A.

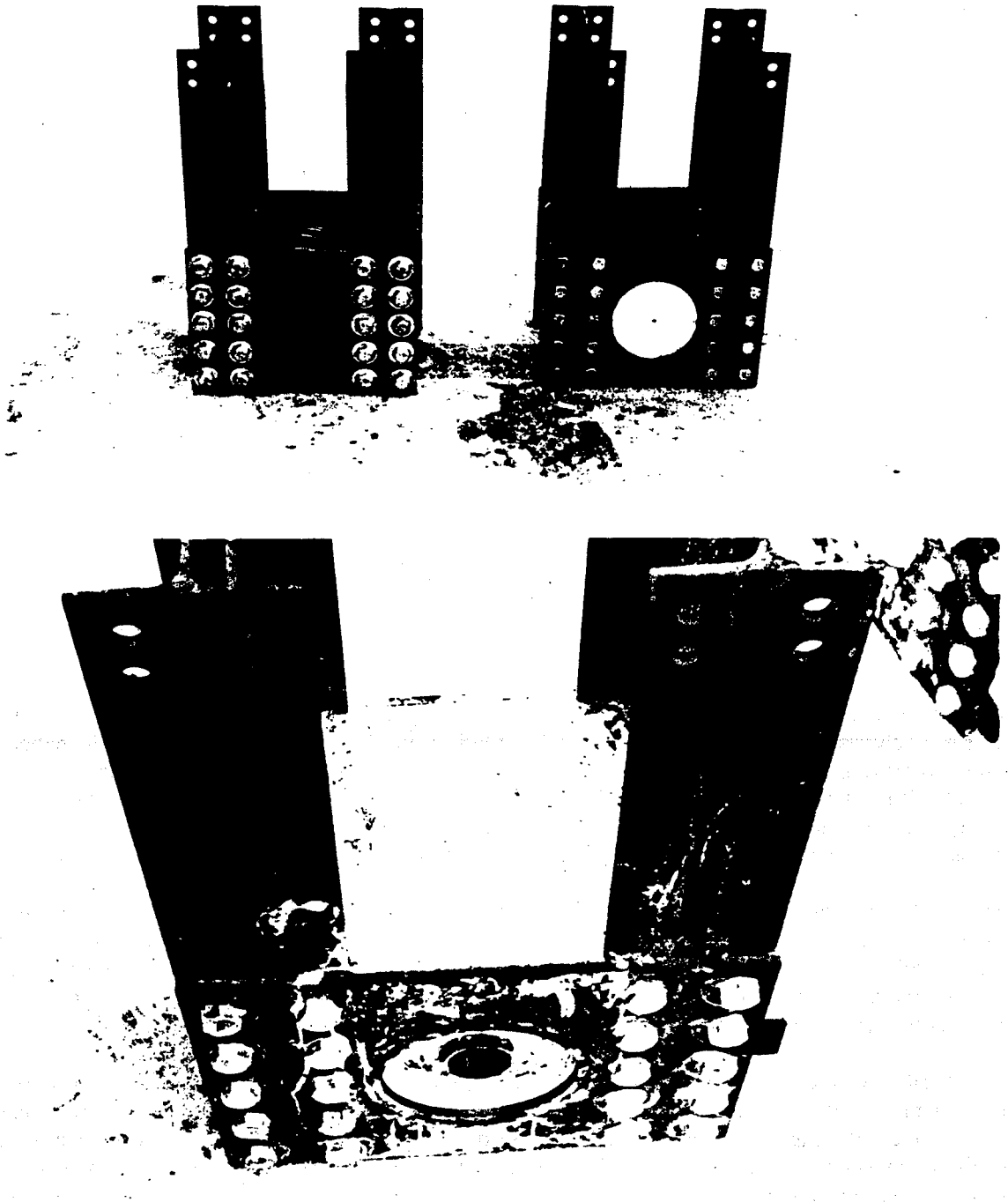

FIGURE 26 Loading block before concreting (*top*) and after concreting (*bottom*).

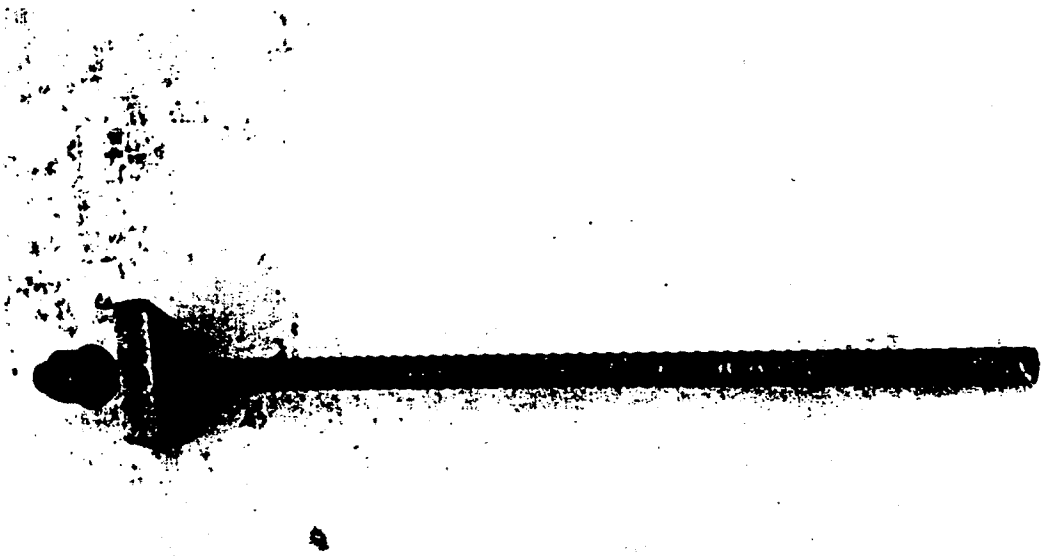

FIGURE 27 Prestressing Dywidag threaded bar with assembly.

EARTHQUAKE APPLICATION OF THE EPF DEVICE

In order to investigate the feasibility of the EPF device for earthquake application, a single freedom subsystem was isolated from a bridge. The system, as shown in Figure 34, consists of a CPUC column, two EPF devices 192 in. apart, foundation, and a torsionally rigid superstructure whose share of weight is 1200 kips on the column. The superstructure is assumed to be torsionally stabilized either at other piers or by its own lateral curvature. For the EPF device, a 21.0-in.-diameter version of the model, whose characteristics are shown in Figure 33, was taken for which the calculated scale factor is 272, and the elastic flexural stiffness is 3,175x272=863,800 k.in. With the given mass and dimensions, this gives a period of oscillation of 1.618 seconds, whose only significance in an inelastic system is that it constitutes an upper limit. Based on the elastic stiffness of the 5,000-psi concrete column of 42.0-in.-diameter without the EPF, the period is 0.337 sec., a ratio of 4.801. In other words, the EPF softens the column and removes it from the range of resonance with earthquake motion.

The calculations were carried out applying the basic differential equation of motion, using no damping other than that resulting from the inelastic stiffness of the EPF devices. The EPF curve, as shown in Figure 35, was converted into a fourth order polynomial, and used for successive approximation of the lateral force and rotation responses of the system. The sinusoidal excitation had a period of 0.480 seconds and an amplitude of acceleration of ±0.4g. This relatively large base motion period was selected to maximize responses.

The rotation reaches a local maximum of 0.0508 rad. and develops EPF moments of 272x88.2=23,990 k.in. In terms of lateral prototype force, this is equivalent to 0.519x0.4x1200 = 249 kips. The normalized lateral force and the corresponding EPF rotations are shown in Figure 36. After passing the local maximum, the curve falls on a straight line parallel to the original tangent, but stops and goes up again as the system is hit by the second wave of positive acceleration. After passing the second local maximum, the response curves fall to –0.0123 rad. and –75.4 k.in., respectively. Thereon, both curves rise again without attaining further local maxima to 1.920 seconds, or a duration of four input cycles, at which time the computation was discontinued.

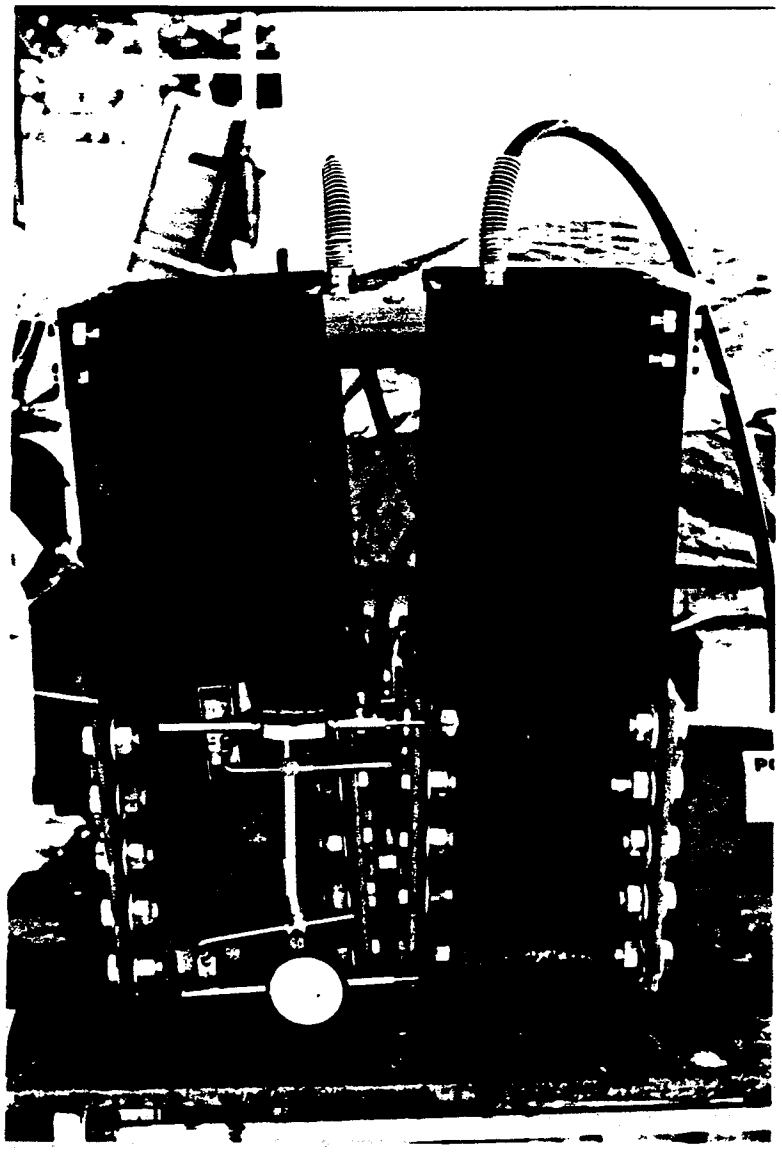

FIGURE 28 Hinge in the compression mode.

As a result of the EPF device alternating between elastic and inelastic modes, both response curves are highly irregular, and do not lend themselves to easy interpretation. The first peak, however, permits certain comparisons with the earthquake provisions of the LRFD Code. The response coefficient C_m, normalized for response modification, is determined as follows:

$$\frac{C_m}{R} = AS\frac{1.2}{T_m^{.33}}$$

where: A = coefficient of acceleration,
S = coefficient for soil type,
T_m = period of fundamental mode of vibration,
R = response modification factor.

If the foundation is solid rock or equal, S=1.0. For single columns of critical graded bridges, R=1.5. With these values, the above equation yields:

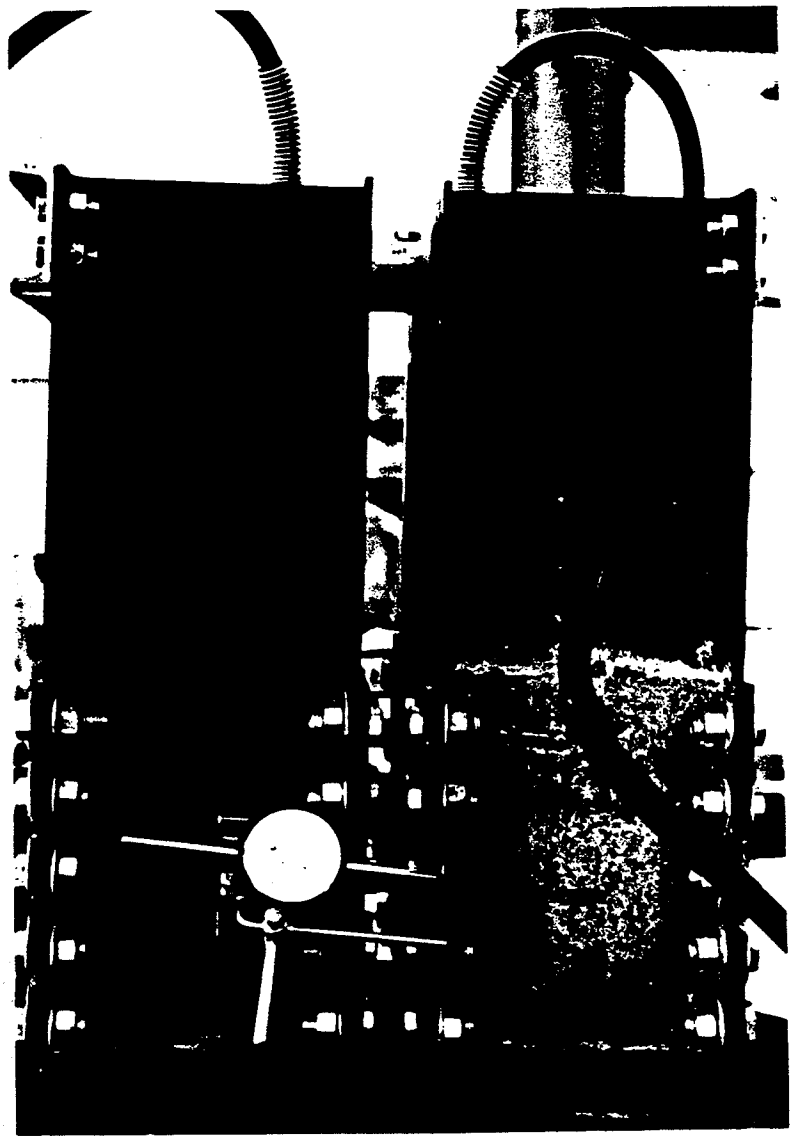

FIGURE 29 Hinge in the tension mode.

for columns without EPF:
T_m=0.337 sec.; C_mR=0.660

for columns with EPF:
T_m=0.618 sec. (min.); C_mR=0.232

The maximum computed response acceleration value from the above analysis is 0.519x0.4=0.208. The close agreement between these two numbers (0.208 and 0.232) is indicative of the numerical correctness of the analysis, and shows that the code value may prove to be directly applicable in the design of columns fitted out with EPF devices. The reduction from 0.660 to 0.208, or 68.5%, is substantial and promises a fundamental structural solution for earthquake problems.

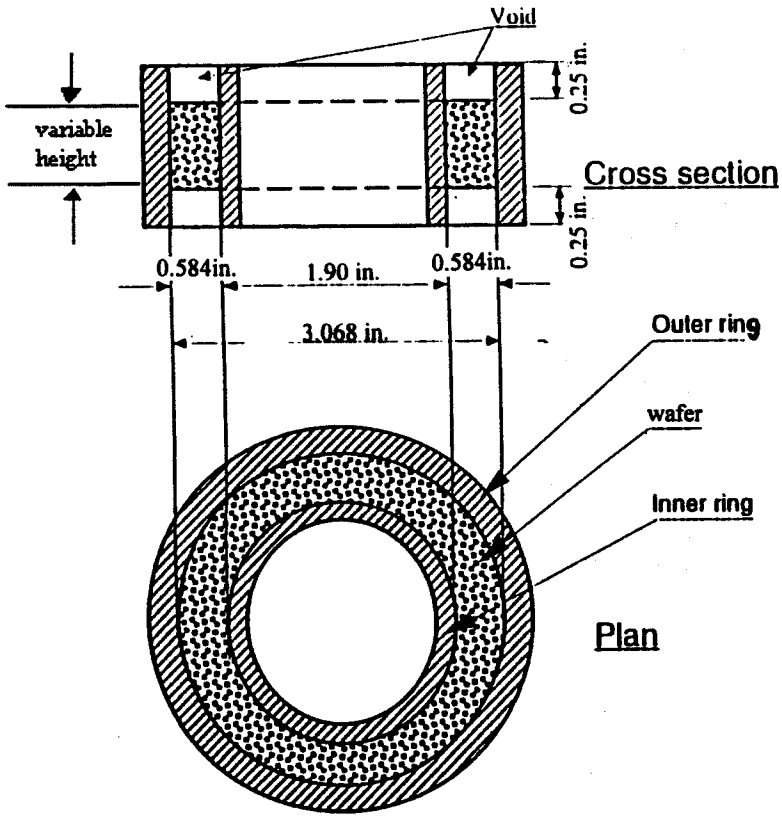

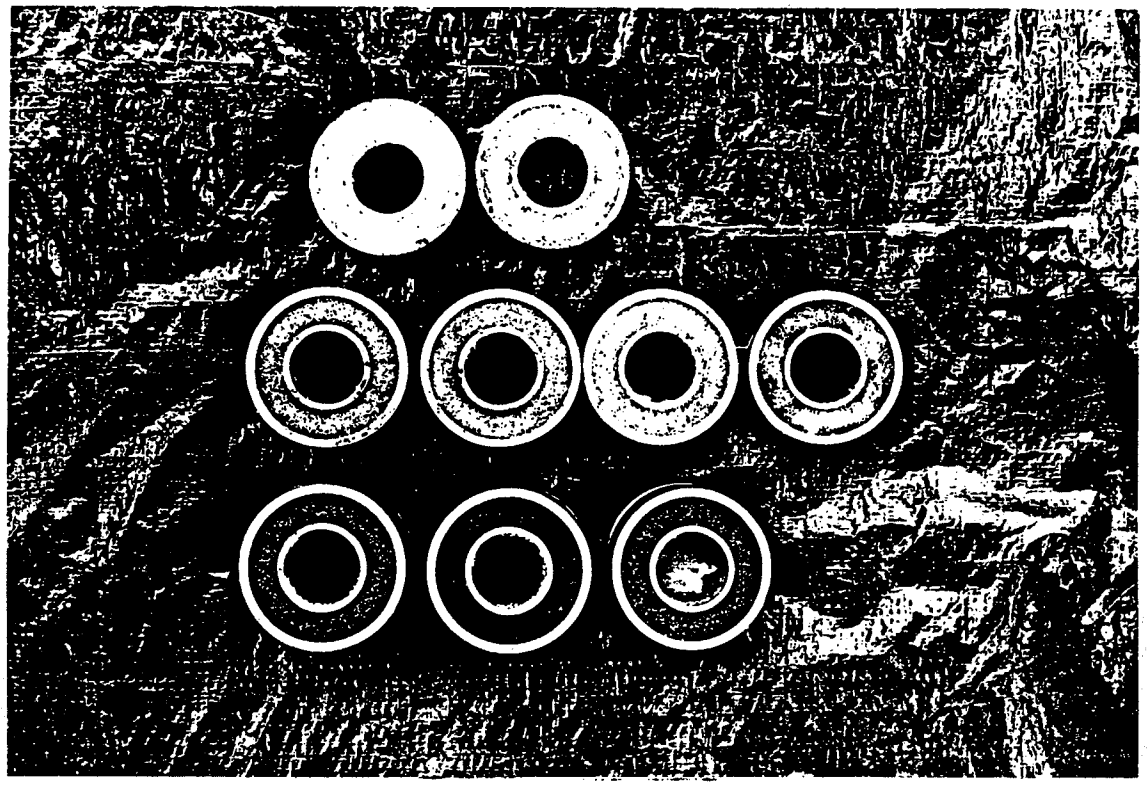

FIGURE 30 ***Top:*** **Hinge details.**
Bottom: **Hinge test specimens.**

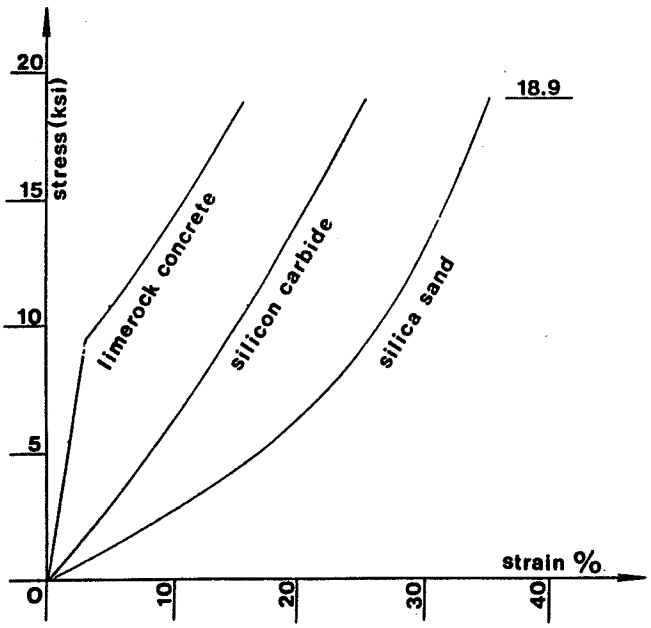

FIGURE 31 Stress-strain under uniform pressure.

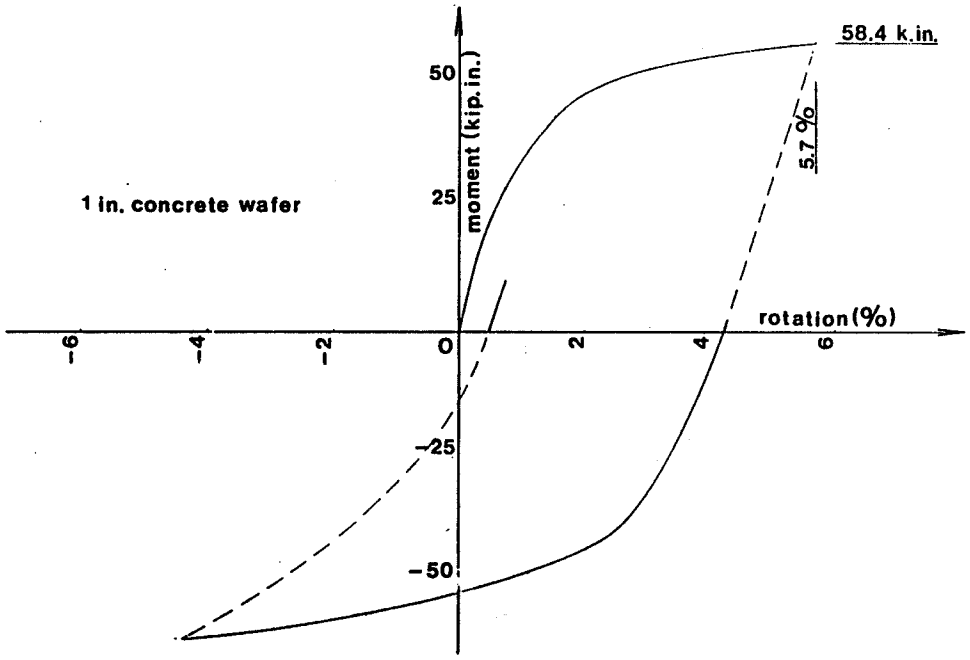

FIGURE 32 First cycle hysteresis curve.

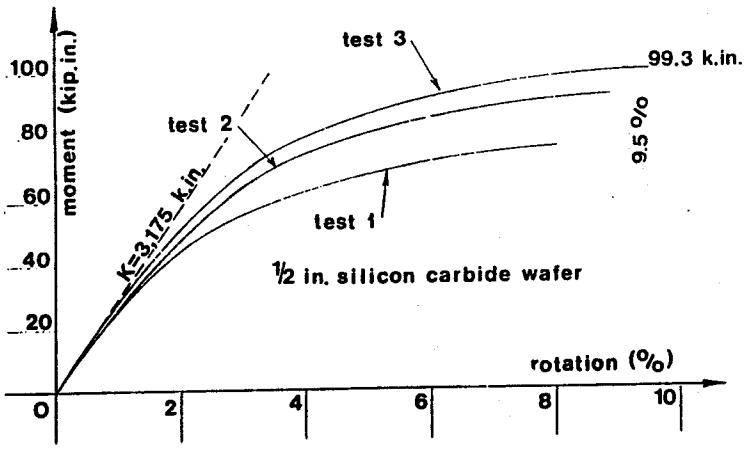

FIGURE 33 Half moment-rotation curve.

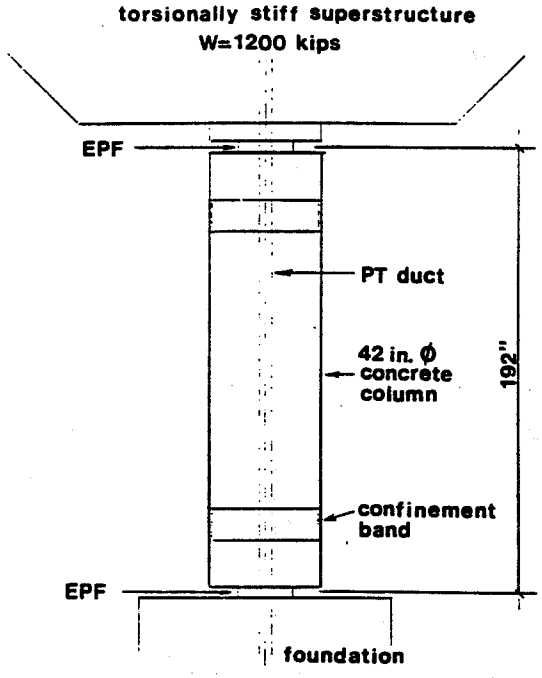

FIGURE 34 A bridge application of EPF.

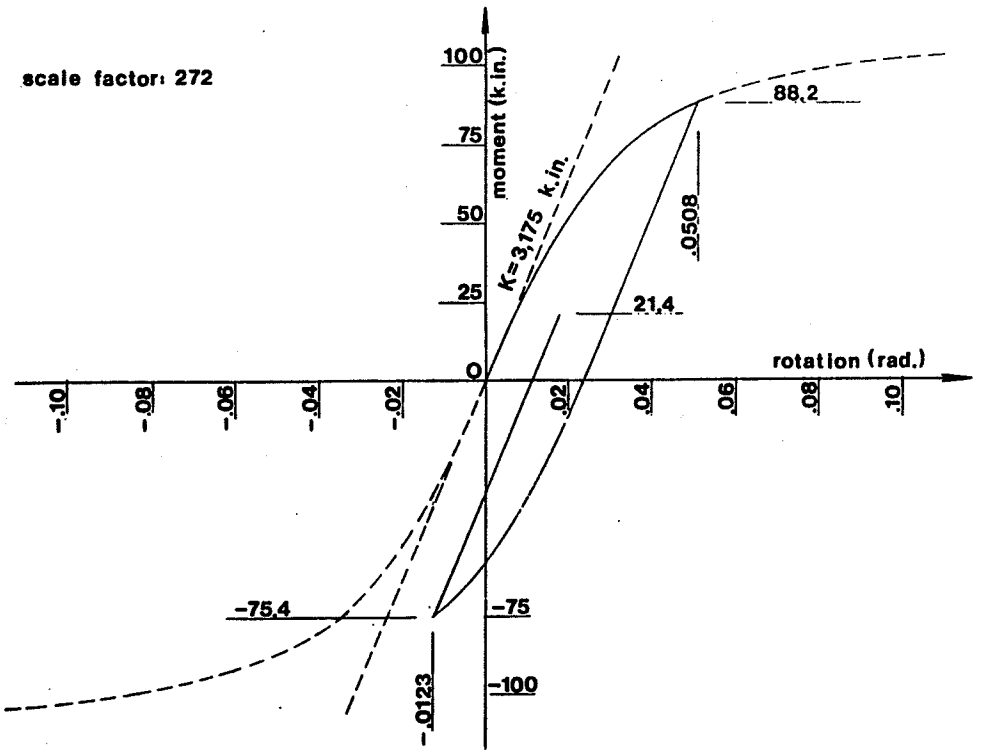

FIGURE 35 EPF moment-rotation curve.

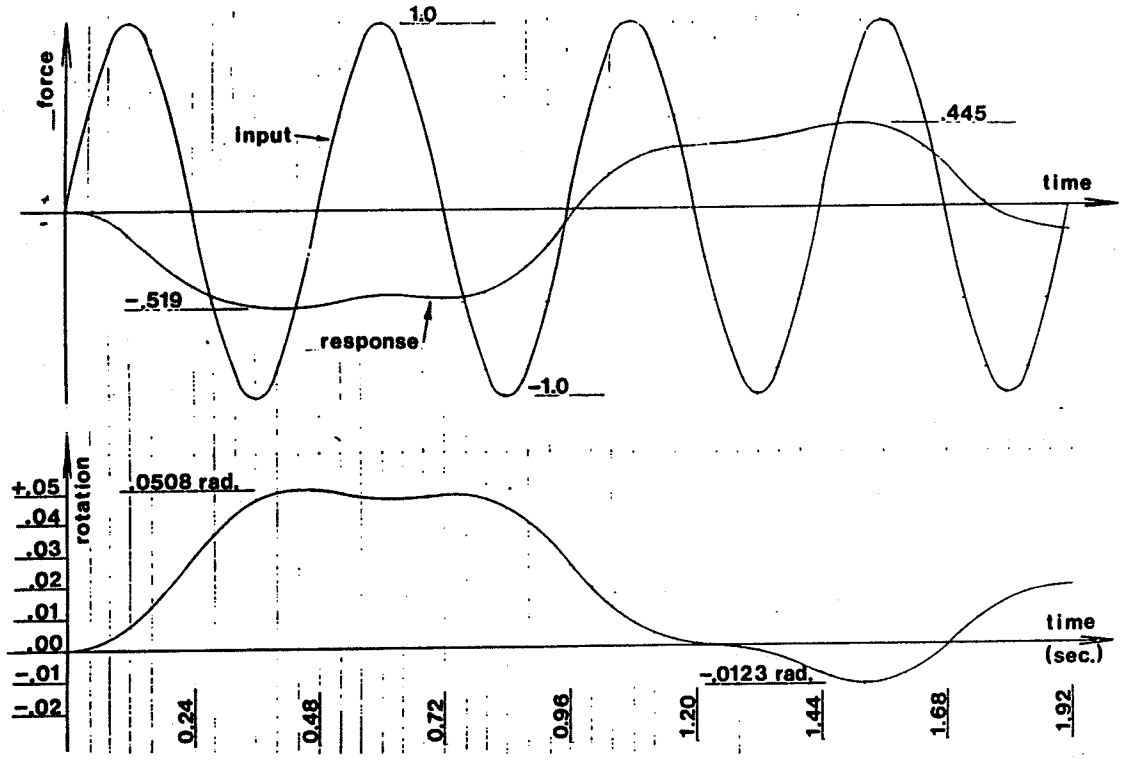

FIGURE 36 EPF response characteristics.

The lateral displacement of the superstructure at the maximum rotation of 0.0508 rad. is 9.75 in., and the corresponding P/Δ moment is 5,850 k.in. Normally, for such a large displacement, the P/Δ effect would be incorporated in the seismic analysis. A direct summation brings the total moment to 29,840 k.in., slightly above the 272x99.3=27,010 k.in. capacity of the 21.0-in.-diameter device. The estimated resistance of a 22.0-in.-diameter device is 31,060 k.in.

The nominal flexural resistance of a 42.0-in.-diameter column, with respect to its center, is 34.730 k.in. In other words, the resistance of the device can be set in such a way that the column itself is protected. Extrapolating from test results, the total compressive force on the device to deliver stated moments is about 3,620 kips, of which 1,200 kips are provided by the weight of the superstructure. The difference would mean a permanent prestress of about 1,750 psi for the 42.0-in. column. Of course, in a prototype design, the prestressing force requirements between the column and the EPF need to be coordinated, and the P/Δ effects of the superstructure weight adequately considered.

In summary, it can be stated that the EPF device is an inexpensive device, made from traditionally used structural materials, which is capable of both mitigating and resisting earthquake-induced force effects in bridges, while protecting the columns against distress.

SUMMARY

PART I

- Compressive failure of concrete is tensile in nature, and likely the result of a yet-to-be-determined interplay between compressive and shear stresses at the fracture plane.
- The angle of fracture plane to the longitudinal axis varies between 15° and 20°, by which various structural fracture mechanisms can plausibly be explained.
- The geometry of the standard compressive test cylinder causes it to produce inflated strength measurements; the error increases with strength.
- The currently used 0.85 strength reduction factor is too conservative.

PART II

For the design of CPUC columns and piles, compressive and cracking service limit states need not be applied. The latter should be replaced by crack-opening limit states for which only permanent loads and imposed deformations need to be considered.

Application of the CPUC column/pile offers the following advantages in comparison with reinforced columns and traditionally prestressed piles:

- requires no transverse reinforcement,
- the absence of transverse reinforcement removes the structural cause for premature spalling of the cover,
- eliminates longitudinal reinforcement and expensive and unreliable splicing thereof,
- eliminates the problem of cover tolerances,
- permits easy and effective compaction of concrete,
- eliminates the compressive incompatibility between steel and concrete in the inelastic phase,
- permits relatively easy analysis in the inelastic phase, including P/Δ effects,
- fully utilizes the strength of concrete,
- has adequate ductility, except for severe earthquake effects,
- turns the column into a multidirectional prestressed beam of high reliability and high attendant resistance factors,
- the increased cover provides adequate corrosion protection for service life, and
- it is economical.

PART III

Application of the EPF device offers the following advantages in comparison with reinforced columns for seismic application:

- reduces seismic force effects by two-thirds by increasing the fundamental period of vibration,
- dissipates energy by inelastic action,
- permits repetitive action without damage to itself or to the adjoining components,
- utilizes traditional structural materials,
- is structurally compatible with the CPUC column,
- acts as a genuine structural component, resists transient loads without excessive deformation, and allows imposed deformations without excessive force effects,
- requires little or no maintenance, and
- is economical.

The EPF device was tailored to be compatible with the CPUC column design. For structural engineers who may feel uncomfortable using the CPUC column for reasons of ductility, collision resistance, etc., the column can be given some traditional reinforcement between the EPF devices, if so desired.

APPENDIX

A.1 RESULTS

Table A.1.1 Results of test 1- Concrete hinge with wafer height of 0.5 in.

Lateral Force kips.	Moment kips. in.	Dial gage reading			Diff. in.	Rotation %
		Top	Center	Bottom		
Cycle I - Condition: Moment jack in compression						
0	0	1.060	.032	.889	---	---
1.33	21.9	1.033	.032	.933	0.071	0.89
2.65	43.8	0.973	.028	.999	0.197	2.46
3.54	58.4	Plastic flow				
Cycle I - Condition: Moment jack in Tension						
0	0	0.842	0.039	1.157	---	---
o.49	8.1	0.864	0.045	1.141	.038	.48
1.18	19.4	0.879	0.048	1.128	.066	.83
1.76	29.1	0.900	0.053	1.110	.105	1.43
2.35	38.8	0.920	0.058	1.092	.143	1.79
2.94	48.5	0.952	0.067	1.060	.207	2.59
3.33	55.0	0.977	0.073	1.033	.259	3.24
3.92	64.7	1.021	0.083	0.982	.351	4.42
4.12	67.9	Plastic flow				
Cycle II - Condition: Moment jack in compression						
0	0	1.072	0.110	0.944	0	--
0.89	14.6	1.046	0.108	0.976	0.058	0.72
1.77	29.2	1.029	0.105	0.994	0.093	1.16
2.66	43.8	0.993	0.100	1.024	0.159	1.99

Table A.1.1 Results of test 1 (continued)

Lateral Force kips.	Moment kips. in.	Dial gage readings			Diff. in.	Rotation %
		Top	Center	Bottom		
3.54	58.4	0.942	0.093	1.068	0.254	3.17
4.42	73	0.757	0.062	1.214	0.585	7.31
Cycle II - Condition: Moment jack in tension						
0	0	0.927	0.106	1.093	---	---
o.69	11.3	0.941	0.109	1.082	.025	.31
1.37	22.6	0.956	0.111	1.071	.051	.64
1.96	32.3	0.970	0.114	1.055	.081	1.01
2.45	40.4	0.984	0.117	1.040	.110	1.37
2.94	48.5	0.996	0.119	1.027	.135	1.69
3.53	58.2	1.016	0.123	1.003	.179	2.24
3.92	64.7	1.036	0.127	0.980	.222	2.77
4.41	72.8	1.059	0.133	0.949	.276	3.45
Cycle III - Condition: Moment jack in compression						
0	0	1.057	0.145	0.951	0	--
0.89	14.6	1.031	0.140	0.984	0.059	0.74
1.77	29.2	1.015	0.138	1.002	0.093	1.16
2.66	43.8	0.993	0.134	1.023	0.136	1.70
3.54	58.4	0.944	0.127	1.061	0.223	2.79
4.42	73	0.829	0.110	1.144	0.421	5.26
4.96	81.8	Plastic flow				

Table A.1.1 Results of test 1 (continued)

Lateral Force kips.	Moment kips. in.	Dial gage readings			Diff. in.	Rotation %
		Top	Center	Bottom		
Cycle III - Condition: Moment jack in tension						
0	0	0.920	0.138	1.090	---	---
o.49	8.1	0.933	0.141	1.078	.025	.31
1.37	22.6	0.948	0.144	1.066	.052	.65
1.96	32.3	0.965	0.142	1.049	.086	1.07
2.45	40.4	0.983	0.149	1.036	.117	1.46
2.94	48.5	0.989	0.151	1.024	.135	1.69
3.53	58.2	1.005	0.155	1.003	.172	2.15
3.92	64.7	1.021	0.159	0.982	.209	2.61
4.41	72.8	1.040	0.163	0.956	.254	3.17
4.70	77.6	1.093	0.178	0.875	.388	4.85
Cycle IV - Condition: Moment jack in compression						
0	0	1.023	0.171	0.975	0	--
0.89	14.6	1.001	0.168	0.999	.046	.57
1.77	29.2	0.983	0.164	1.019	.084	1.05
2.66	43.8	0.961	0.160	1.039	.126	1.57
3.54	58.4	0.910	0.152	1.078	.216	2.70
4.42	73	0.823	0.136	1.143	.368	4.60
4.96	81.8	Plastic flow				

Table A.1.2 Results of test 2- Silica sand hinge with wafer height of 0.5 in.

Lateral Force kips.	Moment kips. in.	Dial gage readings			Diff. in.	Rotation %
		Top	Center	Bottom		
Cycle I - Condition: Moment jack in compression						
0	0	1.156	1.124	1.049	---	---
0.89	14.6	1.134	1.121	1.079	.052	.65
1.77	29.2	1.112	1.118	1.113	.108	1.35
2.66	43.8	1.078	1.113	1.146	.175	2.19
3.54	58.4	0.961	1.099	1.245	.391	4.89
4.43	73.0	Plastic flow				
Cycle I - Condition: Moment jack in Tension						
0	0	1.036	1.122	1.217	---	---
o.69	11.3	1.055	1.126	1.204	.032	.40
1.568	25.9	1.077	1.131	1.184	.074	.92
1.96	32.3	1.091	1.134	1.173	.099	1.24
2.45	40.4	1.107	1.138	1.158	.130	1.62
2.94	48.5	1.129	1.142	1.138	.172	2.15
3.43	56.6	1.147	1.145	1.120	.208	2.60
3.92	64.7	1.184	1.151	1.083	.282	4.65
Cycle II - Condition: Moment jack in compression						
0	0	1.186	1.152	1.091	0	--
0.89	14.6	1.161	1.149	1.118	.052	.65
1.77	29.2	1.144	1.145	1.134	.085	1.06

Table A.1.2 Results of test 2 (continued)

Lateral Force kips.	Moment kips. in.	Dial gage readings			Diff. in.	Rotation %
		Top	Center	Bottom		
2.66	43.8	1.113	1.139	1.164	.146	1.82
3.54	58.4	1.068	1.130	1.199	.226	2.82
4.43	73.0	0.947	1.109	1.286	.434	5.42
5.31	87.6	0.855	1.085	1.356	.596	7.45
Cycle II - Condition: Moment jack in tension						
0	0	1.084	1.140	1.201	---	---
o.98	16.2	1.104	1.145	1.187	.034	.42
1.96	32.3	1.126	1.150	1.174	.069	.86
2.94	48.5	1.149	1.155	1.143	.123	1.54
3.43	56.6	1.162	1.157	1.129	.150	1.88
3.92	64.7	1.178	1.160	1.101	.194	2.42
4.51	74.4	1.204	1.164	1.085	.236	2.95
4.90	80.9	1.229	1.169	1.050	.296	3.70
Cycle III - Condition: Moment jack in compression						
0	0	1.201	1.167	1.088	0	--
0.89	14.6	1.176	1.162	1.115	.052	.65
1.77	29.2	1.153	1.158	1.137	.097	1.21
2.66	43.8	1.131	1.153	1.157	.139	1.74
3.54	58.4	1.096	1.147	1.186	.203	2.53
4.42	73.0	0.991	1.127	1.261	.383	4.79
5.31	87.6	0.878	1.097	1.348	.583	7.28

Table A.1.2 Results of test 2 (continued)

Lateral Force kips.	Moment kips. in.	Dial gage readings			Diff. in.	Rotation %
		Top	Center	Bottom		
Cycle III - Condition: Moment jack in tension						
0	0	1.093	1.151	1.205	---	---
.98	16.2	1.116	1.156	1.184	.021	.55
1.96	32.3	1.136	1.160	1.164	.041	1.05
2.94	48.5	1.161	1.165	1.138	.067	1.69
3.92	64.7	1.185	1.170	1.112	.093	2.31
4.51	74.4	1.205	1.173	1.094	.111	2.79
4.90	80.9	1.223	1.176	1.065	.140	3.37
5.39	88.9	1.270	1.185	0.998	.207	4.80

Table A.1.3 Results of test 3-Carborunrum hinge with wafer height of 0.5 in.

Lateral Force kips.	Moment kips. in.	Dial gage readings			Diff. in.	Rotation %
		Top	Center	Bottom		
Cycle I - Condition: Moment jack in compression						
0	0	1.038	0.251	0.928	---	---
0.89	14.6	1.010	0.251	0.965	.065	.80
1.77	29.2	0.985	0.250	0.992	.113	1.50
2.66	43.8	0.926	0.244	1.053	.237	3.00

Table A.1.3 Results of test 3 (continued)

Lateral Force kips.	Moment kips. in.	Dail gage readings			Diff. in.	Rotation %
		top	Center	Bottom		
3.54	58.4	0.865	0.231	1.120	.365	4.60
4.43	73.0	0.773	0.212	1.195	.532	6.70
5.31	87.6	0.674	0.188	1.277	.713	8.90
Cycle I - Condition: Moment jack in tension						
0	0	0.900	0.249	1.130	---	---
.98	16.2	0.930	0.256	1.104	.056	.70
1.96	32.3	0.972	0.262	1.078	.124	1.55
2.94	48.5	1.028	0.270	1.034	.224	2.80
3.92	64.7	1.059	0.273	1.009	.280	3.50
4.41	72.8	1.091	0.277	0.981	.340	4.25
4.90	80.9	1.154	0.283	0.919	.465	5.81
5.10	84.2	1.205	0.286	0.869	.566	7.08
Cycle II - Condition: Moment jack in compression						
0	0	1.018	0.294	0.974	0	--
0.89	14.6	0.989	0.292	1.000	.055	.70
1.77	29.2	0.964	0.290	1.024	.104	1.30
2.66	43.8	0.936	0.286	1.049	.157	2.00
3.54	58.4	0.874	0.275	1.099	.269	3.40
4.42	73.0	0.776	0.255	1.176	.444	5.60
5.31	87.6	0.698	0.237	1.234	.580	7.31
5.66	93.5	Plastic flow				

Table A.1.3 Results of test 3 (continued)

Lateral Force kips.	Moment kips. in.	Dail gage readings			Diff. in.	Rotation %
		Top	Center	Bottom		
Cycle II - Condition: Moment jack in tension						
0	0	0.900	0.278	1.139	---	---
.98	16.2	0.931	0.284	1.114	.056	.70
1.96	32.3	0.962	0.289	1.091	.110	1.40
2.94	48.5	0.990	0.292	1.069	.160	2.10
3.92	64.7	1.022	0.295	1.038	.223	2.80
4.90	80.9	1.067	0.299	0.996	.310	3.90
5.39	88.9	1.107	0.301	0.955	.391	4.90
5.88	97.0	1.162	0.302	0.898	.503	6.30
Cycle III - Condition: Moment jack in compression						
0	0	1.073	0.307	0.998	0	--
0.89	14.6	1.038	0.304	1.029	.066	.80
1.77	29.2	1.019	0.302	1.047	.103	1.20
2.66	43.8	0.987	0.298	1.075	.163	2.00
3.54	58.4	0.927	0.287	1.121	.269	3.40
4.42	73.0	0.836	0.270	1.187	.426	5.30
5.31	87.6	0.745	0.247	1.255	.585	7.31
6.20	102.2	Plastic flow				

Table A.1.3 Results of test 3 (continued)

Lateral Force kips.	Moment kips. in.	Deformations			Diff. in.	Rotation %
		Top	Center	Bottom		
Cycle III - Condition: Moment jack in tension						
0	0	0.943	0.290	1.136	---	---
.98	16.2	0.973	0.297	1.112	.054	.70
1.96	32.3	0.998	0.300	1.091	.100	1.30
2.94	48.5	1.020	0.303	1.071	.142	1.80
3.92	64.7	1.049	0.306	1.043	.199	2.50
4.90	80.9	1.085	0.309	1.003	.275	3.40
5.39	88.9	1.104	0.310	0.981	.316	4.00
5.88	97.0	1.140	0.311	0.941	.392	4.90

Table A.1.4 Results of test 4 -Concrete hinge with wafer height of 1.0 in.

Lateral Force kips.	Moment kips. in.	Dial gage readings			Diff. in.	Rotation %
		Top	Center	Bottom		
Cycle: I Condition: Moment jack in compression						
0	0	1.070	1.022	0.991	---	---
.89	14.6	1.062	1.022	1.004	.021	.26
1.77	29.2	1.045	1.021	1.021	.055	.69
2.66	43.8	1.014	1.023	1.057	.122	1.52
3.54	58.4	0.820	1.049	1.197	.456	5.70

Table A.1.4 Results of test 4 (Continued)

Lateral Force kips.	Moment kips. in.	Dial gage readings			Diff. in.	Rotation %
		Top	Center	Bottom		
Cycle I - Condition: Moment jack in tension						
0	0	0.890	1.087	1.146	---	---
.98	16.2	0.911	1.094	1.126	.041	.51
1.96	32.3	0.936	1.100	1.097	.095	1.19
2.94	48.5	0.960	1.108	0.969	.247	3.09
3.43	59.6	1.096	1.149	0.899	.453	5.66
3.72	61.4	1.204	1.166	0.775	.685	8.56
Cycle II - Condition: Moment jack in compression						
0	0	1.072	1.185	1.030	---	---
.89	14.6	1.036	1.188	1.063	.069	.86
1.77	29.2	1.007	1.190	1.087	.122	1.52
2.66	43.8	0.970	1.191	1.115	.187	2.34
3.54	58.4	0.923	1.195	1.147	.266	3.32
4.43	73.0	0.694	1.195	1.303	.651	8.14
Cycle II - Condition: Moment jack in tension						
0	0	0.906	1.236	1.055	---	---
1.18	19.4	0.940	1.245	1.022	.067	.84
1.96	32.3	0.965	1.249	0.996	.118	1.47
2.94	48.5	0.999	1.256	0.956	.192	2.40
3.43	59.6	1.013	1.258	0.939	.223	2.79
3.92	64.7	1.040	1.263	0.903	.286	3.57

Table A.1.4 Results of test 4 (Continued)

Lateral Force kips.	Moment kips. in.	Dial gage readings			Diff. in.	Rotation %
		Top	Center	Bottom		
4.41	72.8	1.107	1.271	0.826	.430	5.37
Cycle III - Condition: Moment jack in compression						
0	0	1.061	1.282	0.901	---	---
.89	14.6	1.017	1.283	0.942	.085	1.06
1.77	29.2	0.997	1.284	0.959	.122	1.52
2.66	43.8	0.953	1.283	0.991	.198	2.47
3.54	58.4	0.914	1.283	1.019	.265	3.31
4.43	73.0	0.850	1.282	1.060	.370	4.62
Cycle III - Condition: Moment jack in tension						
0	0	0.940	1.305	1.006	---	---
.98	16.2	0.970	1.308	0.979	.057	.71
1.96	32.3	1.004	1.311	0.947	.123	1.54
2.94	48.5	1.035	1.314	0.913	.188	2.35
3.92	64.7	1.063	1.317	0.879	.250	3.12
4.41	72.8	1.094	1.319	0.840	.320	4.00
4.90	80.9	1.150	1.322	0.776	.440	5.50

Table A.1.5 Results of test 5- Concrete hinge with wafer height of 1.5 in.

Lateral Force kips.	Moment kips. in.	Dial gage readings			Diff. in.	Rotation %
		Top	Center	Bottom		
Cycle I - Condition: Moment jack in compression						
0	0	0.829	0.176	0.766	---	---
.89	14.6	0.804	0.174	0.809	.068	.90
1.77	29.2	0.774	0.169	0.862	.151	1.90
2.66	43.8	0.727	0.158	0.939	.275	3.40
3.54	58.4	0.680	0.105	1.154	.537	6.70
Cycle I - Condition: Moment jack in tension						
0	0	0.737	0.154	1.048	---	---
.98	16.2	0.766	0.159	1.029	.048	.60
1.96	32.3	0.796	0.164	1.008	.099	1.20
2.94	48.5	0.865	0.197	0.925	.251	3.10
3.92	64.7	plastic flow				
Cycle II - Condition: Moment jack in compression						
0	0	0.923	0.280	0.837	---	---
.89	14.6	0.900	0.281	0.860	.046	.60
1.77	29.2	0.875	0.280	0.887	.098	1.20
2.66	43.8	0.842	0.276	0.920	.164	2.10
3.54	58.4	0.769	0.264	1.000	.317	4.00
3.89	64.3	plastic flow				

Table A.1.5 Results of test 5 (Continued)

Lateral Force kips.	Moment kips. in.	Dial gage readings			Diff. in.	Rotation %
		Top	Center	Bottom		
Cycle II - Condition: Moment jack in tension						
0	0	0.842	0.282	0.962	---	---
.98	16.2	0.869	0.289	0.935	.054	.68
1.96	32.3	0 890	0.294	0.908	.102	1.28
2.94	48.5	0.918	0.303	0.872	.166	2.08
3.92	64.7	Further readings not available (Dial gage needle slipped)				
Cycle III - Condition: Moment jack in compression						
0	0	0.904	0.321	0.860	---	---
.89	14.6	0.879	0.318	0.887	.052	.70
1.77	29.2	0.862	0.314	0.905	.087	1.10
2.66	43.8	0.836	0.309	0.930	.138	1.70
3.54	58.4	0.803	0.302	0.964	.205	2.60
4.25	70.0	0.628	0.258	1.147	.563	7.00
Cycle I - Condition: Moment jack in tension						
0	0	0.812	0.314	1.012	---	---
.98	16.2	0.834	0.319	0.994	.040	.50
1.96	32.3	0.859	0.324	0.971	.088	1.10
2.94	48.5	0.881	0.329	0.946	.135	1.70
3.92	64.7	0.908	0.337	0.911	.197	2.50
4.41	72.8	0.923	0.342	0.891	.232	2.90
4.51	74.4	plastic flow				

A.2 CUMULATIVE ROTATIONS

Table A.2.1 Cumulative rotations for concrete hinge with wafer height of 0.5 in.

Moment - kips. in.	Net deformation - in.	Rotation -%
Cycle I: Compression		
0	0	0
21.92	0.071	0.89
43.8	0.197	2.46
--	--	--
Cycle I: Tension		
0	0.218	2.73
-8.1	0.18	2.25
-19.4	0.152	1.90
-29.1	0.101	1.26
-38.8	0.075	0.94
-48.5	0.011	0.14
-55	-0.041	-0.51
-64.7	-0.136	-1.70
----	----	----
Cycle II: Compression		
0	-.225	-2.81
14.6	-.167	-2.09
29.2	-.132	-1.65
43.8	-.066	-.83
58.4	0.029	0.36
73.0	0.360	4.50

Table A.2.1 Cumulative rotations (continued)

Moment - kips. in.	Net deformation - in.	Rotation -%
Cycle II: Tension		
0	0.069	0.86
-11.3	0.044	0.55
-22.6	0.018	0.23
-32.3	-0.012	-0.15
-40.4	-0.041	-0.51
-48.5	-0.066	-0.83
-58.2	-0.110	-1.38
-64.7	-0.153	-1.91
-72.8	-0.207	-2.59
Cycle III: Compression		
0	-0.203	-2.54
14.6	-0.144	-1.80
29.2	-0.110	-1.38
43.8	-0.067	-0.84
58.4	0.02	0.25
73.0	0.218	2.75
Cycle III: Tension		
0	0.073	0.91
-8.1	0.048	0.60
-22.6	0.021	0.26
-32.3	-0.013	-0.16
-40.4	-0.044	-0.55

Table A.2.1 Cumulative rotations (continued)

Moment - kips. in.	Net deformation - in.	Rotation -%
-48.5	-0.062	-0.78
-58.2	-0.099	-1.24
-64.7	-0.136	-1.70
-72.8	-0.181	-2.26
-77.6	-0.315	-3.94
Cycle IV: Compression		
0	-0.145	-1.81
14.6	-0.099	-1.24
29.2	-0.061	-0.76
43.8	-0.019	-0.24
58.4	0.071	0.89
73.0	0.223	2.79

Table A.2.2 Cumulative rotations for carborundum hinge with wafer height of 0.5 in.

Moment - kips. in.	Net deformation - in.	Rotation -%
Cycle I: Compression		
0	0	0
14.6	0.065	0.80
29.2	0.118	1.50
43.8	0.237	3.00
58.4	0.365	4.60
73.0	0.532	6.70

Table A.2.2 Cumulative rotations (continued)

Moment - kips. in.	Net deformation - in.	Rotation -%
87.6	0.713	8.90
Cycle I: Tension		
0	0.340	4.30
-16.17	0.284	3.55
-32.34	0.216	2.70
-48.51	0.116	1.45
-64.68	0.06	0.75
-72.77	0	0
-80.85	-0.125	-1.56
-84.08	-0.226	-2.83
Cycle II: Compression		
0	0.066	0.83
14.60	0.121	1.50
29.21	0.170	2.13
43.81	0.223	2.79
58.41	0.335	4.19
73.01	0.510	6.38
87.62	0.646	8.08
Cycle II: Tension		
0	0.349	4.36
-16.17	0.293	3.66
-32.34	0.239	2.99
-48.51	0.189	2.36

Table A.2.2 Cumulative rotations (continued)

Moment - kips. in.	Net deformation - in.	Rotation -%
-64.68	0.126	1.58
-80.85	0.039	0.49
-88.94	-0.042	-0.53
-97.02	-0.154	-1.90
Cycle III: Compression		
0	0.035	0.44
14.6	0.101	1.26
29.2	0.138	1.73
43.8	0.198	2.48
58.4	0.304	3.80
73.0	0.461	5.76
87.6	0.620	7.75
Cycle III: Tension		
0	0.303	3.79
-16.17	0.249	3.11
-32.34	0.203	2.54
-48.51	0.161	2.01
-64.68	0.104	1.30
-80.85	0.028	0.35
-88.94	-0.013	-0.16
-97.02	-0.089	-1.11

Table A.2.3 Cumulative rotations for silica sand hinge with wafer height of 0.5 in.

Moment - kips. in.	Net deformation - in.	Rotation -%
Cycle I: Compression		
0	0	0
14.6	0.052	0.70
29.2	0.108	1.40
43.8	0.175	2.20
58.4	0.391	4.90
---	---	---
Cycle I: Tension		
0	0.288	3.60
-11.3	0.256	3.20
-25.9	0.214	2.68
-32.2	0.189	2.36
-40.4	0.158	1.98
-48.5	0.116	1.45
-56.6	0.08	1.00
-64.7	0.06	0.75
Cycle II: Compression		
0	0.066	0.83
14.6	0.118	1.48

Table A.2.3 Cumulative rotations (continued)

Moment - kips. in.	Net deformation - in.	Rotation -%
29.2	0.151	1.89
43.8	0.212	2.65
58.4	0.292	3.65
73.0	0.500	6.25
Cycle II: Tension		
0	0.278	3.48
-16.2	0.244	3.05
-32.2	0.209	2.61
-48.5	0.155	1.94
-56.6	0.128	1.60
-64.0	0.084	1.05
-74.4	0.042	0.53
-80.8	-0.018	-0.23
Cycle III: Compression		
0	0.048	0.60
14.6	0.100	1.25
29.2	0.145	1.81
43.8	0.187	2.34
58.4	0.251	3.14
73.0	0.431	5.39
87.6	0.631	7.89
Cycle III: Tension		
0	0.273	3.41

Table A.2.3 Cumulative rotations (continued)

Moment - kips. in.	Net deformation - in.	Rotation -%
-16.2	0.229	2.86
-32.2	0.189	2.36
-48.5	0.138	1.73
-64.7	0.088	1.10
-74.4	0.050	0.63
-80.8	0.003	0.04
-88.9	-0.111	-1.39

Table A.2.4 Cumulative rotations for concrete hinge with wafer height of 1.0 in.

Moment - kips. in.	Net deformation - in.	Rotation -%
Cycle I: Compression		
0	0	0
14.6	0.021	0.26
29.2	0.055	0.69
43.8	0.122	1.52
58.4	0.456	5.70
Cycle I: Tension		
0	0.335	4.19
-16.2	0.294	3.67
-32.3	0.240	3.00

Table A.2.4 Cumulative rotations (continued)

Moment - kips. in.	Net deformation - in.	Rotation -%
-48.5	0.088	1.10
-56.6	-0.118	-1.47
-61.4	-0.350	-4.37
Cycle II : Compression		
0	0.037	0.46
14.6	0.106	1.32
29.2	0.159	1.99
43.8	0.224	2.80
58.4	0.303	3.79
73.0	0.688	8.60
Cycle II : Tension		
0	0.288	2.85
-19.4	0.161	2.01
-32.3	0.110	1.37
-48.5	0.036	0.45
-56.6	0.005	0.06
-64.7	-0.058	-0.72
-72.8	-0.202	-2.52
Cycle III: Compression		
0	-0.081	-1.01
14.6	0.004	0.05
29.2	0.041	0.51
43.8	0.117	1.46

Table A.2.4 Cumulative rotations (continued)

Moment - kips. in.	Net deformation - in.	Rotation -%
58.4	0.184	2.30
73.0	0.289	3.61
Cycle III: Tension		
0	0.145	1.81
-16.2	0.088	1.10
-32.2	0.022	0.27
-48.5	-0.043	-0.54
-64.7	-0.105	-1.31
-72.8	-0.175	-2.19
-80.8	-0.295	-3.69

A.3 MOMENT-ROTATION CURVES

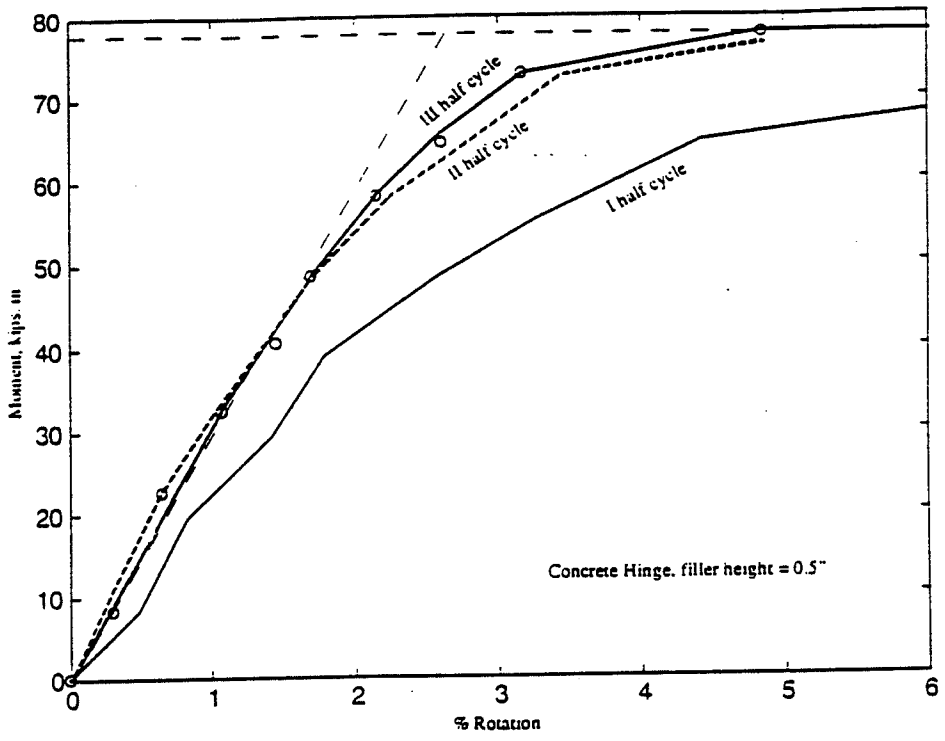

a. Tension mode

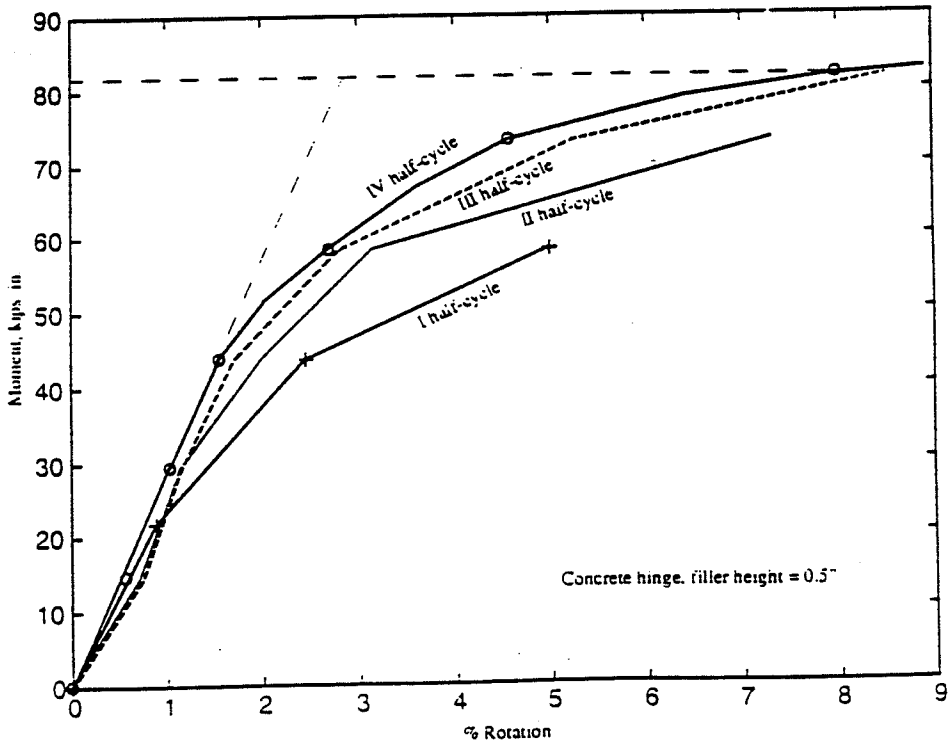

b. Compression mode

FIGURE A.3.1 Moment-Rotation Curves for Concrete Hinge

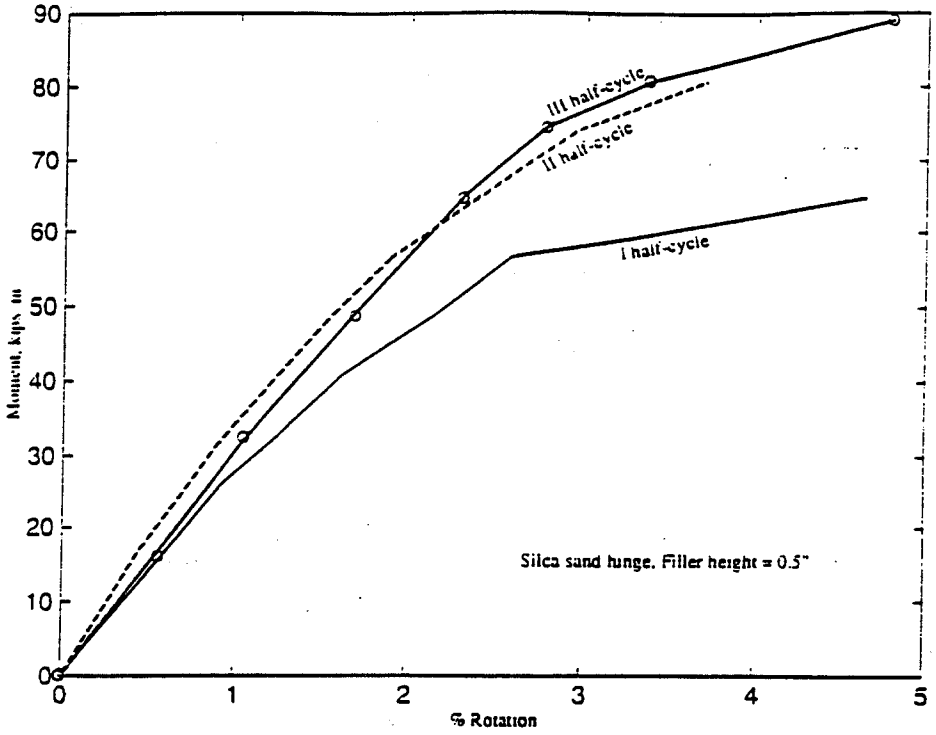

a. Tension mode

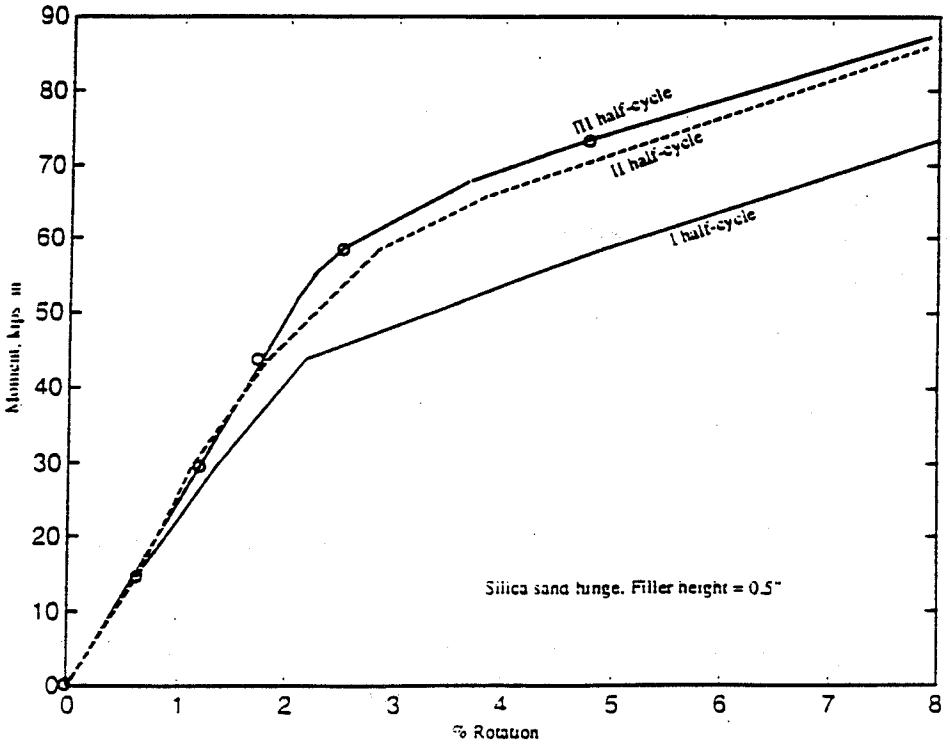

b. Compression mode

FIGURE A.3.2 Moment-Rotation Curves for Silica Sand Hinge

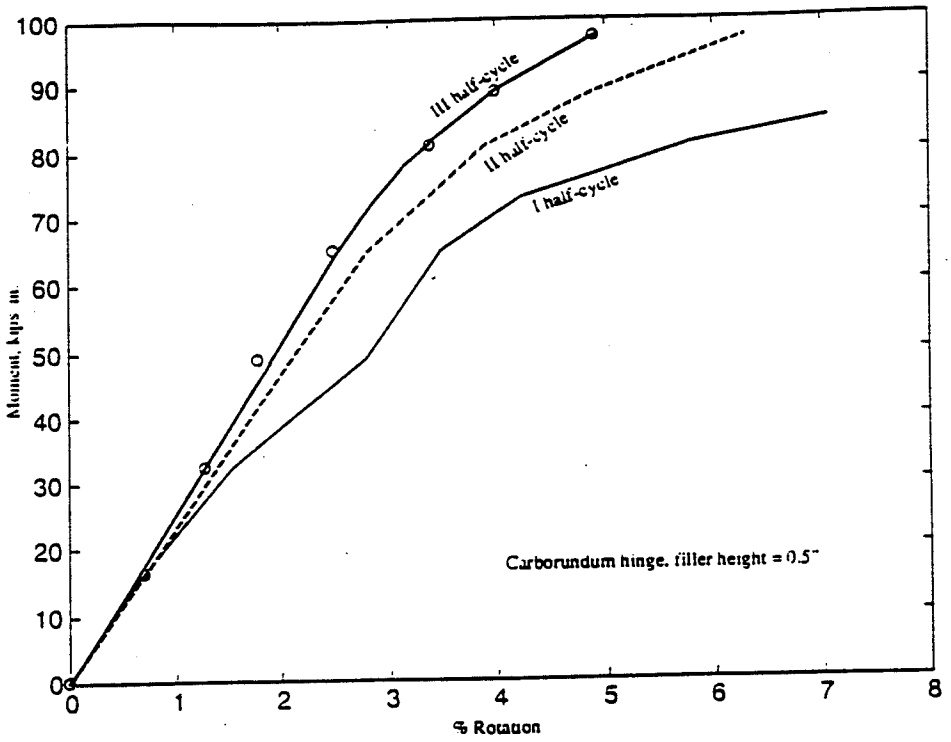

a. Tension mode

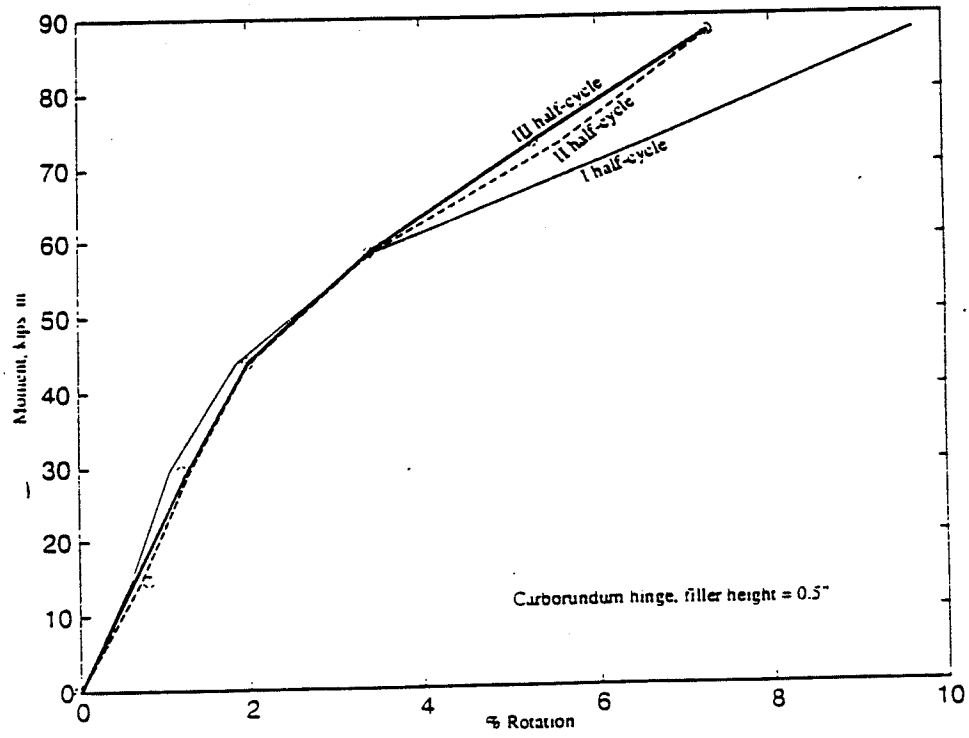

a. compression mode

FIGURE A.3.3 Moment-Rotation Curves For Caborundum Hinge

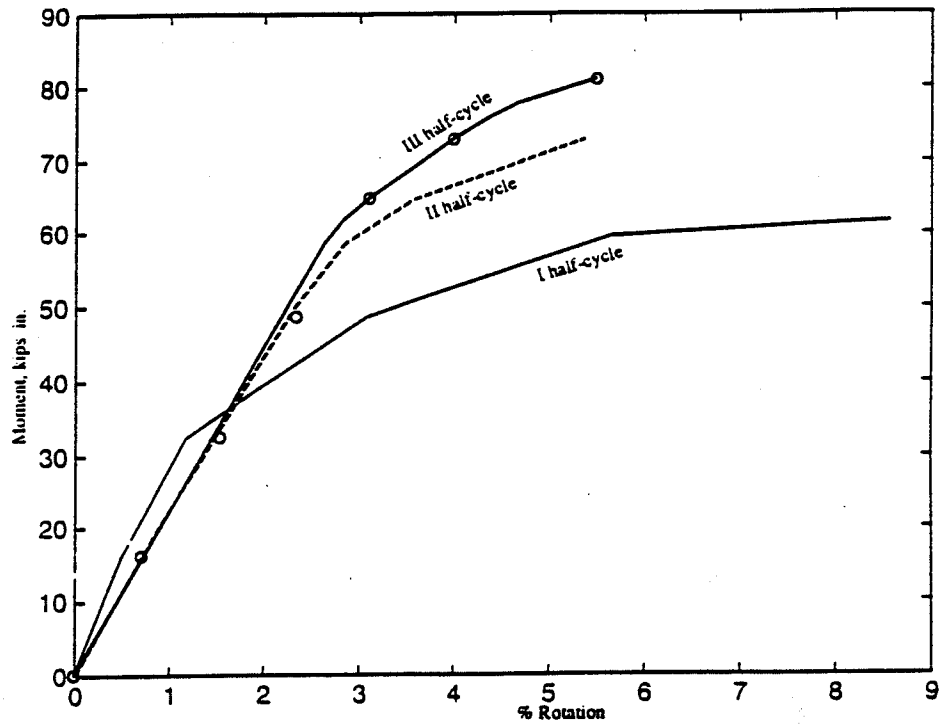

a. Tension mode

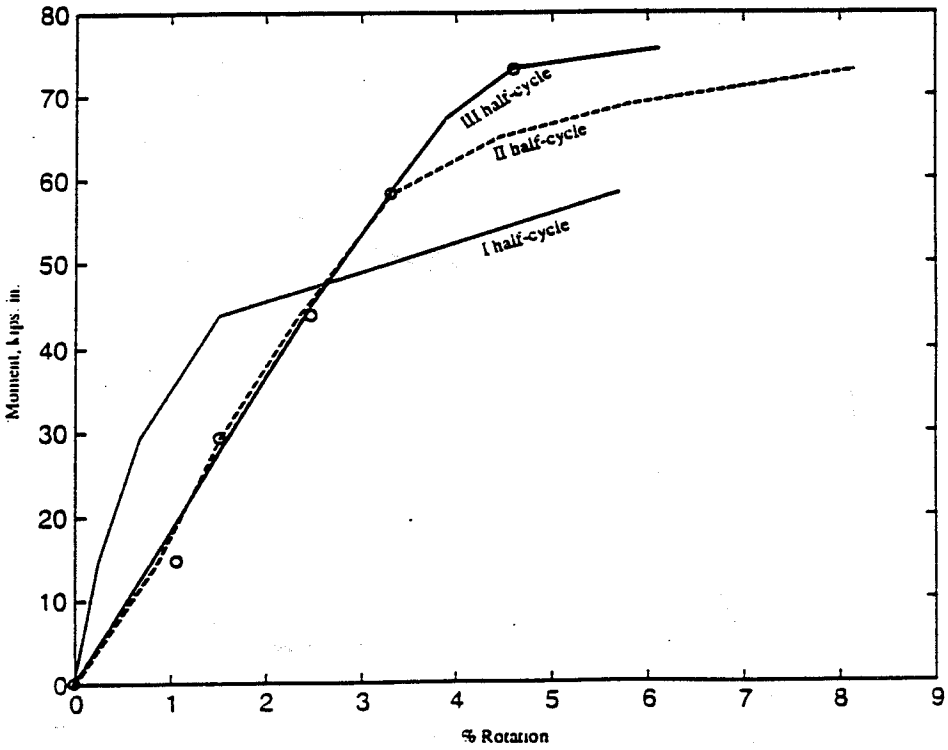

b. Compression mode

FIGURE A.3.4 Moment-Rotation Curves For Concrete Hinge with Filler Height of 1.0in.

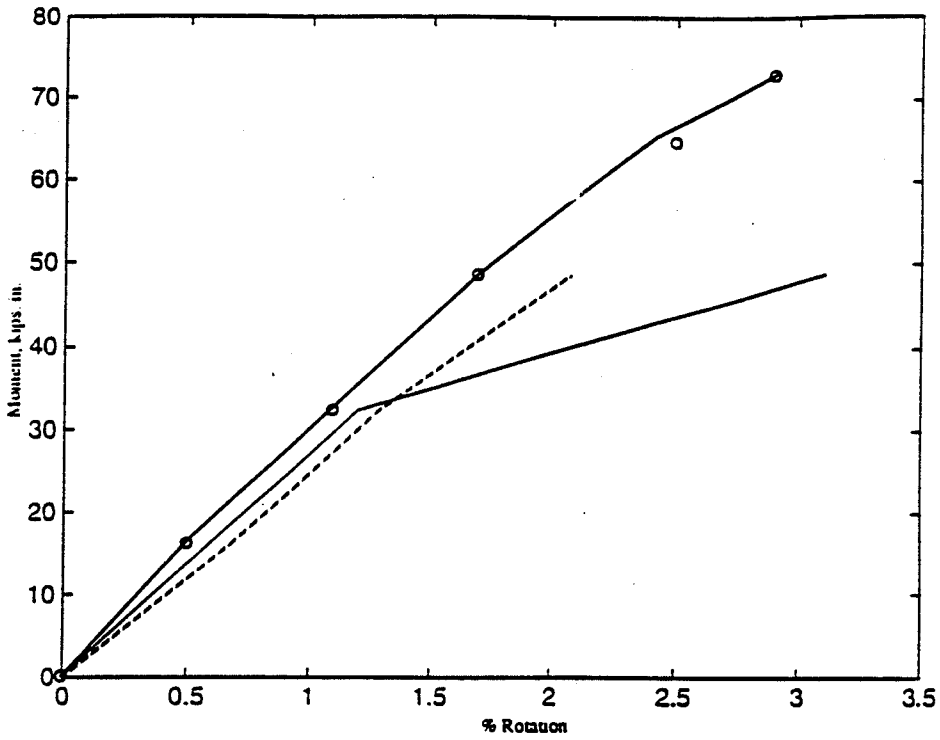

a. Tension mode

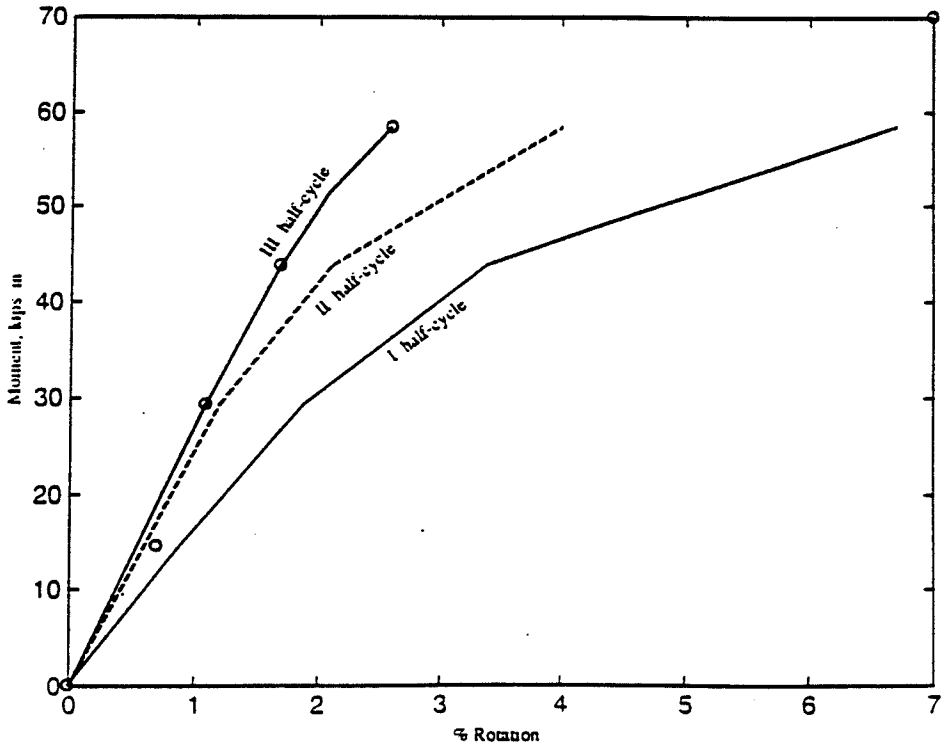

b. compression mode

FIGURE A.3.5 Moment-Rotation Curves For Concrete Hinge with Filler Height of 1.5in.

ACKNOWLEDGEMENT

The Principal Investigators would like to thank the Transportation Research Board (Project NCHRP-94-ID014) for their generous financial support. Gratitude is expressed to the following persons and companies for their valuable input and guidance:

Anthony Garcia; Wingerter Lab, Inc., Miami; Florida Wires and Cables, Inc.; Florida Steel Corp.; W.R. Grace & Co.; Mr. Rathinam Periyaiah; Mr. P. Clark; Mr. G.E. Hankison; Mr. G.S.V. Prasad, Mr. T. Frazier, Mr. W. Ahn, Mr. D. Knut, Mr. F. Navarette, Mr. G. Gervois, Mr. K.A. Allady, and other graduate assistants from Florida Atlantic University; Ms. Barbara Larkin; Dr. L.A. Carlsson; Dr. S.E. Dunn; and Dr. C.S. Hartley.